Chapter 19
Quantum Dots as Optical Materials: Small Wonders and Endless Frontiers

Sisir K. Sarkar

19.1 Introduction

The current lifestyle has embraced optics and photonics technologies in various ways spanning from communication, computation, energy sector, medical science, to entertainment. The last decade has witnessed advances in optical fiber communications, which led to a 100-fold increase in the amount of communicable information enabling a society-transforming internet to blossom. Charles Kao pronounced in his 2009 Nobel Prize lecture that our present daily lives have been transformed by fiber communication. Truly such communications have enabled us to visualize a "flat world" and the present internet would not have existed without optics (National Academies Press 2013).

The year 2015 celebrated the International Year of Light (IYL) and light-based technologies for promoting sustainable development to global challenges in energy, education, agriculture, health care, and security. In the last decade, advances in transmitting information, on the one hand, have enabled internet service, and on the other hand, provided the displays on our smartphones and computing devices. This is surely a promising trend for the world's economy.

Optics affecting energy conservation globally is best exemplified by the invention of light-emitting diodes (LEDs) for lighting purposes. Another prominent development is to create white light by combining blue LEDs based on gallium nitride (GaN) with fluorescent phosphors containing rare earth elements like europium and terbium. Synthetic biology has emerged as a new amazing field. This has helped genetically engineered specific optical properties to be incorporated into living organisms and effectively produce optically active materials.

Materials are playing a significant role in the technological evolution catering to new types of solar cells, sensors, and imaging of cellular functions. It is known

S. K. Sarkar (✉)
Bhabha Atomic Research Center, Mumbai 400085, India
e-mail: sisirchhaya@gmail.com

R. S. Ningthoujam and A. K. Tyagi (eds.), *Handbook of Materials Science, Volume 1*,
Indian Institute of Metals Series, https://doi.org/10.1007/978-981-99-7145-9_19

from the literature that the pace of material development has always been a slow albeit costly process. But, with the rise of awareness of the importance of certain materials and advent of engineered materials, material research has assumed strategic significance. These days, key optoelectronic materials are playing a significant role in negotiations between countries.

In recent years, low-dimensional materials having strong nonlinear optical properties such as quantum dots (QDs) and core–shell quantum dots (CSQDs), have been the subject of intense research and development. Novel materials like II–VI group semiconductor quantum dots exhibit size and shape-dependent various physicochemical properties, which led to many fascinating application areas in optoelectronics, sensors, and medicines (Tong and Wang 2020; Efros and Brus 2021). Cadmium selenide, CdSe, is a vital member of this group having band gap energy, E_g of 1.75 eV at room temperature. Since this band gap matches well with the solar energy spectrum, the flexibility to tune its optoelectronic properties make them a very useful material (Peng et al. 2005).

The current synthetic methods employ rigorous conditions of temperature, pressure, passive atmosphere, toxic reducing agents, etc. However, a one-step synthesis method employing the electron beam (EB) has provided a simple efficient green method. Herein, the synthesis of CdSe quantum dot (QD) in homogeneous (water) as well as in microheterogeneous systems (water-in-oil microemulsions, ionic liquid) using EB irradiation was reported (Singh et al. 2013a).

Next, advance in this area centered on core–shell architecture, which provided an efficient approach for QDs' surface passivation. In this architecture, the robust shell effectively isolate the core QDs from the adjoining environment and suppress the formation of surface defects/traps. Besides, by appropriately selecting the core and shell materials, it is possible to control the band structure of such core–shell QDs (CSQD). The desired nonlinear optical properties can be achieved by varying the size/shape, and chemical composition of core and shell materials. In this overview, some of the interesting optical properties of QDs, as well as of CSQDs are assessed, such as nonlinear refraction, optical limiting, saturable absorption, reverse saturable absorption, etc. Various tailored optoelectronic devices including solar cells, light-emitting diodes, optical switch/limiter, QD laser, and biological/chemical applications are discussed. These successes have maintained the momentum of this subject area catering to a wide-ranging group of scientists and technologists to work for future prospective applications, which are conversed at the end (Huang et al. 2020).

The expression "optics and photonics" stated above is actually the manifestation of light's dual nature (i) a propagating electromagnetic wave, and (ii) a collection of traveling particles called photons, with similar impact potential like electronics. The best examples of these enablers are laser and associated burgeoning activities. At this point, it may be briefly stated that laser is a source of light that can be (i) coherent, meaning that a group of photons can act as a single unit, and (ii) monochromatic, meaning that the photons can have a well-defined single color. Subsequently, some more often-used terms like optics, electro-optics, optoelectronics, and photonics are described in the literature (Brown and Pike 1995).

Optics, the science of light, is based on several ideas like transmission of light, principle of least time, and well-known law of refraction. These ideas were consequently reinforced in nineteenth century by several path-breaking discoveries such as interference of light (Hooke, Young, Boyle), diffraction (Grimaldi, Fresnel), polarization (Huygens), corpuscular theory (Newton), and, undoubtedly, by Maxwell's theory on electromagnetic fields. End of this century ushered in the age of quantum optics practically ending the field of classical optics. Max Planck introduced the concept of light quanta, marking the beginning of quantum theory. With the invention of the first ruby laser in 1960, many apparently detached principles forwarded by Einstein, Bose, and others were systematized.

The terms "Electro-optics" and "optoelectronics" describe the interaction of light with electrical fields. John Kerr in 1875 established that the refractive index of materials is a function of an electric field. However, the "electro-optics" term became popular in the literature only by the early 1960s and a society called "Lasers and Electro-Optics Society" was formed in 1985 thus legitimizing the name professionally. The field of "optoelectronics" seems to be a subfield of electro-optics studying electronic devices for making source, detection, and control of light. Commonly, "optoelectronics" term refers to the quantum effects of light on semiconductor materials. Electron multiplication in Si and Ge p-n junctions were demonstrated in 1953 and then semiconductors started gaining importance in optics. Subsequently, Neumann indicated the possibility of building a semiconductor laser amplifying the stimulated emission of radiation.

The term "photonics" started appearing in literature around 1981 through reports from Bell Laboratories and Hughes Aircraft Corporation. The renowned International Society for Optics and Photonics (SPIE) organized in 1995 a huge conference in optics and photonics where photonics was showcased as the "engineering applications of light." It was involved in the detection, transmission, storing, process information, display, and generation of energy. However, presently, photonics and optics have become synonymous in the technical literature. Interestingly, based on this development, the "Lasers and Electro-Optics Society" also changed its name to "IEEE Photonics Society" in 2008.

19.2 Back to Basics: Big Excitement by Working Small

The genesis of nanotechnology is associated with two events: first, the famous lecture entitled "There's plenty of room at the bottom" by Nobel Laurate Richard Feynman at the American Physical Society meeting in 1959 (Feynman 1960), and secondly, the talk "On the basic concept of Nanotechnology" by Norio Taniguchi at the International Conference on Production Engineering in Tokyo in 1974 (Taniguchi 1974). Feynman predicted that one day, researchers will have just the right size tools for directly manipulating atoms and molecules.

This was a historic prediction in which Feynman forecasted the creation and modification of materials at a fundamental level besides reworking on nature's products. But, scientists have to wait till the last few decades to start directly working in this strange world. The excitement of working in this nano regime rests on the different behavior of materials at ultra-small levels. It is possible to control the materials' fundamental properties like color, melting temperature, hardness, conductivity, strength, etc., (Montanarella and Kovalenk 2022; Pietryga et al. 2016) at nanometer-scale structures.

Comparing the dimensions of an atom (10^{-10} m), a nanoscale material is essentially an assembly of a few atoms or molecules. Over the years, scientists have explored the properties of micrometer-sized bulk substances. It was shown, of late, that material properties become dependent on its size and shape (1–100 nm). New properties are perceived due to a lack of symmetry at the interface or electron confinement at the nanometer scale. Thus, properties of collections of atoms or molecules at the nanoscale are different from the individual constituents and also the bulk. The total fraction of atoms on the nanoparticle surface increases with decreasing the size of the particle and can be estimated by the relation: $P = 4\ N^{-1/3} \times 100$, where P is the percentage of surface atoms versus N, the total number of atoms in the particle. One can have better insight by taking an example of a 3 nm iron particle, which has 50% of its atoms on the surface, whereas 10 and 30 nm particles have just 20% and 5% atoms on the surface, respectively. Since the properties depend instead on the nature of the material, on the size, a single material can provide a consistent and continuous range of properties. Typically, gold and silver nanostructures have absorption in the visible region, while CdSe quantum dots of different sizes can have emissions covering the whole visible region.

In 1980, Russian Physicist Ekimov working at the Vavilov State Optical Institute discovered QDs in solids (glass crystals) (Ekimov et al. 1980). In late 1982, the same phenomenon was discovered by American Chemist Brus at Bell Laboratories while working with colloidal solutions (Rossetti et al. 1983). As the crystal grew over a period of days, a change in the wavelength of absorbed or emitted light was observed. This phenomenon was conceptualized in the framework of electron confinement ascribing the quantum mechanical nature of the particle.

QDs are mostly used in all kinds of applications requiring precise control of colored light. As an illustration, when a thin filter made of quantum dots fixed on top of an LED lamp, one can obtain light from a redder shade to a blueish color. Quantum dots are now replacing conventional pigments, dyes, and hi-tech reflective paints, and by embedding in another matrix, incoming light of one color can be emitted as entirely different color light.

Valence electrons of bulk phase semiconductors excited to a higher energy conduction band, energy difference being the band gap, relaxes to its ground state by emitting a photon equivalent to band gap energy. A typical semiconductor quantum dot has a core encircled by a layer of organic ligands (Fig. 19.1a) (Shiang et al. 1995). The stacking of atoms in a representative 20 nm QD consisting of 100,000 atoms is presented in Fig. 19.1b (Shiang et al. 1995).

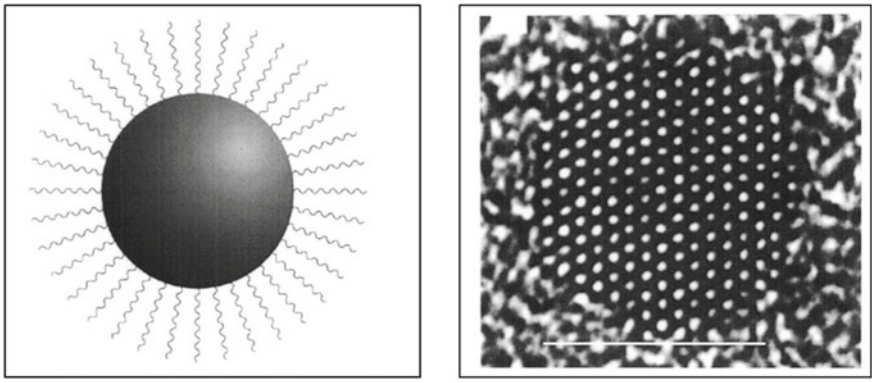

Fig. 19.1 **a** Schematics of a QD with a core (2–20 nm) and a passivating organic ligand shell. **b** High-resolution TEM image of a CdSe nanocrystal showing the array of atoms. Reproduced with permission from ACS Publications (Shiang et al. 1995)

As pointed out already, the optical properties of QDs are heavily dependent on their size. This size dependence was first observed with QD grown by molecular beam epitaxy method. 2D quantum wells having thickness comparable to the Bohr exciton radius, modifies the density of states with fewer band edge states and shifts the bandgap toward blue. Further investigations were continued to make one-dimensional (1D) quantum wires/rods and zero-dimensional (OD) quantum dots. As the QD size gets smaller than the Bohr exciton radius, the photo-excited carriers experience the boundary. This leads to discrete electronic states converting the continuous density of states of the bulk. Figure 19.2 presents the quantum confinement effect in the transition from bulk (3D) materials to quantum dots (0D). Thus, QDs are termed as "artificial atoms" and the quantum dot problem can treated as "particle-in-a-sphere" model. It is shown in the figure that strong confinement results in higher bandgap energy, which in turn shifts the prospective photoluminescence toward blue (Fig. 19.3).

The principle of size-dependent tunability is illustrated in Fig. 19.3a while such tunability of absorption is shown in Fig. 19.3b for the well-studied CdSe quantum dot. It can be seen that the first absorption feature gets red-shifted as the size becomes larger. It is to be noted that the corresponding photoluminescence (PL) always follows the same trend as in emission. Russian researchers used this level-quantization effect in QDs to modify the color of glasses by controlling the size of QDs in silicate glasses. They used a combination of CdSe and CdS QDs put into silicate glasses to produce a range of colors from red to yellow. In the last few decades, synthesis strategies were developed to get precise control of QDs' sizes to make the process commercial, and M/s Quantum Dot Corporation, USA started selling QD products in 1998. Many advanced applications started appearing in the market revolutionizing the industries of display, solar cells, and health care, especially in cancer treatment (Efros and Brus 2021).

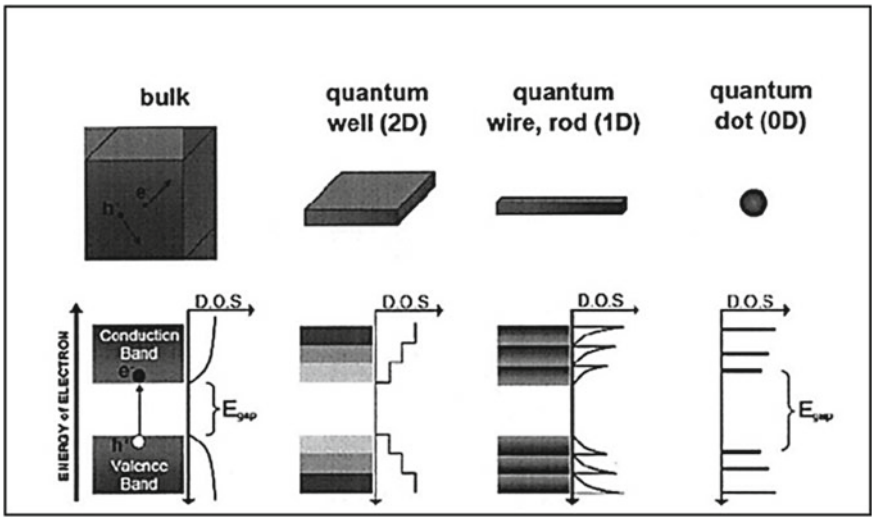

Fig. 19.2 Quantum confinement effect in transition from bulk (3D) materials to quantum dots (0D). Atom-like states are generated owing to confinement in all three dimensions. Reproduced from PhD Thesis (Steckel 2006)

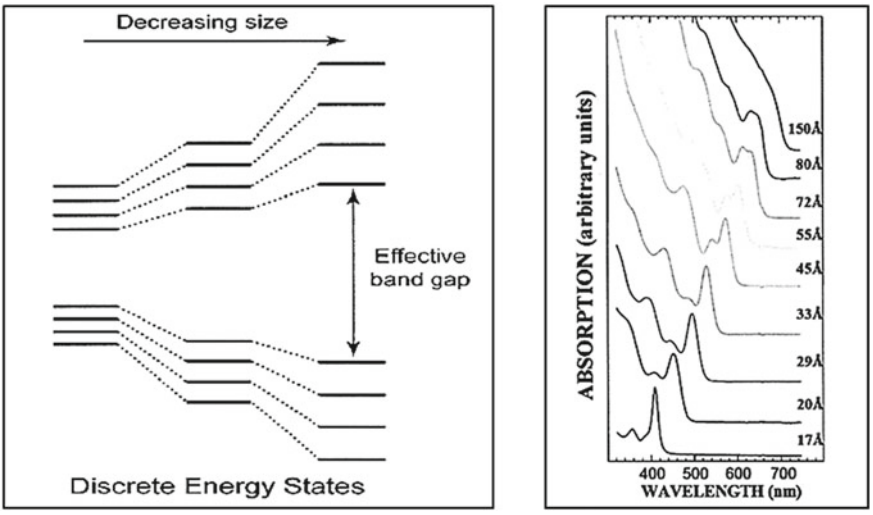

Fig. 19.3 **a** Principle of the size-tunability for QDs. Decrease in size increases the splitting of states and **b** absorption spectra for 2–15 nm CdSe nanocrystals. Reproduced from PhD Thesis (Yen 2007)

M/s Sony advanced the first display in 2013 employing CdSe quantum dots. It improved the backlighting of light-emitting diode (LED) for LCD televisions achieving better color range. Following this, QD-based displays started appearing in the market and M/s Samsung pioneered the upmarket displays acquiring QD Vision in 2016 under the brand "QLED" (using InP instead of CdSe) (Dai et al. 2017). Soon, such displays are expected to infiltrate the market, where quantum dots will be used as color filters/converters. Further, they are also working on the combination of QLED with organic-LED technologies (Palomaki 2022). QDs are expected to play a central role in developing micro-LEDs, flexible displays, and electroluminescent displays (Yang et al. 2021). Besides, researchers are also engaged in developing infrared emitting quantum dots for commercial deployment. M/s Quantum Solutions, currently selling the colloidal materials (i.e., PbS nanocrystals) and M/s Ember ion, has started putting them in infrared cameras and many solid-state devices. Judging from overall rapid deployments, nanotechnology is expected to play a crucial role in the next-generation devices useful in medicine (Shi et al. 2017; Bobo et al. 2016) and photonics (Novotny and Hecht 2006; Mohamed et al. 2021).

With this comprehensive discussion of the basic concept, we now venture into the areas of synthesis, characterization, and applications of QD first and then of CSQD. We will finally explore the future developmental issues and usages of upcoming QD-based optoelectronic devices (Huang et al. 2020).

19.3 Synthesis of QD in Batch Reactors

The motivation for chemical synthesis in solution-phase is to develop a large-scale robust method for producing QDs. It should be pointed out that term "large-scale synthesis" is a comparative concept, where some authors report the production of several grams while others several hundreds of grams. However, a robust large-scale synthesis method should operate under mild conditions with ease of scaling up irrespective of the yield in one batch process.

First, we will take up various batch processes involving hot-injection organometallic synthesis, aqueous synthesis, and biosynthesis approaches. Further, in this context, work is described toward developing a one-step efficient green synthesis method using an electron beam (EB). Using this methodology, CdSe quantum dots (QDs) are synthesized in homogeneous (aqueous) and also in microheterogeneous systems (water-in-oil microemulsions and ionic liquid) and they are characterized by the proven instrumental techniques. The radiolytic processes are shown to proceed through the reactions facilitated by hydrated electrons (e_{aq}^-). Elegant pulse radiolysis technique is used to investigate the formation dynamics of these nanoparticles. Later, a few continuous methods for reproducible large-scale production of QDs are discussed.

19.3.1 Hot-Injection Method

A customary batch reaction pioneered by Murray et al. (1993) for the synthesis of QDs is accomplished by rapidly injecting semiconductor precursors into a hot solvent and organic ligand system. A typical setup is shown in Fig. 19.4 (Murray 1995).

The formation of QDs goes through three stages. First, the reactive monomers are formed by rapid decomposition of the precursors and the monomer concentration continues to grow till a critical supersaturation occurs. This induces energetic nucleation and such nucleation surge lowers the monomer concentration relieving the supersaturation partially. In the intervening time, the existing concentration ensures growth onto the nascent nuclei. When monomer concentration becomes very low due to the continuous reaction depletion, Oswald ripening occurs. Small particles start to dissolve for compensating the growth of large particles and eventually, the growth gets defocused. High-quality, monodisperse QD samples are produced by purposefully controlling the reaction in the growth-focusing region, by adjusting the precursor's amount, the growth time, and multiple injections to keep relatively high monomer concentrations. The relatively high temperature (~300 °C) annealing was found to remove surface trap states following which PL intensity is enhanced. Annealing is believed to first carry out rearranging of semiconductor material and organic ligands at the surface leading to fewer surface trap states. This is also found to passivate the surface and increase the PL efficiency. In subsequent sections, we will have an in-depth discussion on CSQD (Sect. 19.9).

The established technique of solvent/nonsolvent extraction is done repeatedly to obtain the QDs from their original growth solution. Typically, the addition of methanol-induced flocculation of nanocrystals and butanol was added to mix the growth solution with methanol. Precipitated materials are further processed by

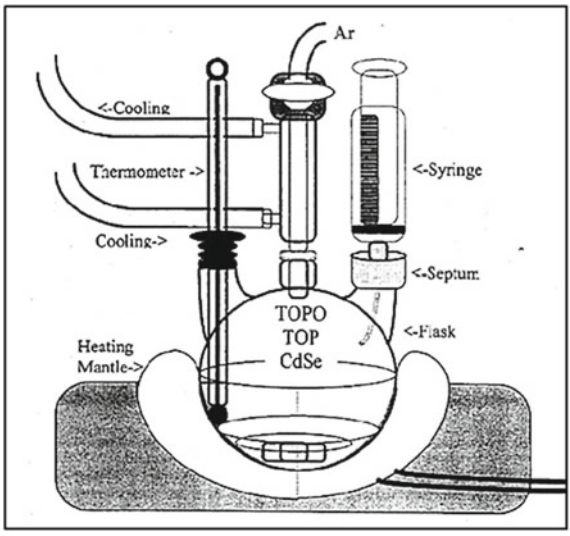

Fig. 19.4 Schematics of a hot-injection organometallic synthesis of CdSe quantum dot. Reproduced with PhD Thesis (Murray 1995)

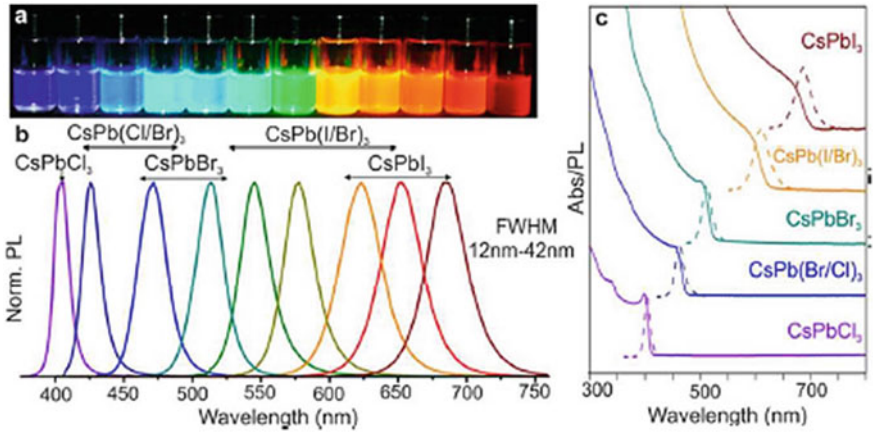

Fig. 19.5 Illustration of narrow and bright emission from perovskite $CsPbX_3$ QDs (X = Cl, Br, I) covering the entire visible region; **a** with UV lamp illumination ($\lambda = 365$ nm); **b** fluorescence spectra on excitation with 400 nm, and 350 nm for $CsPbCl_3$; **c** optical absorption and fluorescence spectra. Reproduced with permission from ACS Publications under Creative Common License (Protesescu et al. 2015)

centrifugation and dispersed in hexane. This method is also good for size-selective precipitation, by gently adding a limited amount of non-solvent (methanol).

Working with appropriate sources and synthetic parameters (Abe et al. 2013), this technique has been extended to a large variety of semiconductor QDs, such as PbS, PbSe, InP, Ag_2S, and $Ag_2S_xSe_{1-x}$. Of late, the interesting all inorganic highly luminescent perovskite QDs $CsPbX_3$ (X = Cl, Br, I) has been synthesized by injecting cesium oleate precursor solution into PbX_2 (X = Cl, Br, I) solution (Protesescu et al. 2015). The fluorescence properties (Fig. 19.5) of as-prepared perovskite QDs have comparable high luminescence of CdSe QDs. Further, Wang et al. (2016) have developed a facile solution-phase hot injection method for shape-controlled production of lead-free and stable single-crystalline perovskite derivative Cs_2SnI_6 QDs.

19.3.2 Aqueous Synthesis

The hot-injection organometallic synthesis usually requires additional phase transfer steps in water for producing QDs required in biological and clinical applications. It is worth mentioning that the disposal of a large volume of organic solvents used in large-scale production pose environmental hazards. To alleviate these issues, work was initiated on aqueous synthesis which has proved to be a potential alternative to the organometallic routes. This aqueous synthesis is also considered to be a green

process offering several advantages: (1) surface functionalization required for biological applications, can be done during the synthesis step and (2) lower reaction temperatures (usually <100 °C). Incidentally, water-based synthesis was attempted in the early 1980s, when CdS QDs were prepared.

Later, Vossmeyer et al. prepared QDs by aqueous synthesis approach using $Cd(ClO_4)\cdot 6H_2O$, H_2S, and 1-thioglycerol. This work reported the size-dependent UV–visible absorption spectra of CdS QD but did not mention any photoluminescence data (Vossmeyer et al. 1994). The first photoluminescence investigation through this route was published by Weller and coworkers (1996) on CdTe QDs. The CdTe QDs were made by refluxing a mixture of Cd^{2+} with NaHTe at 96 °C for several hours. Following this, aqueous synthesis route became popular and many II–VI QDs, such as CdTe, CdSe, HgTe, CdHgTe, and PbS, were synthesized. Later, this route witnessed several advances such as hydrothermal synthesis, microwave irradiation, and ultrasonic treatment. Recently, Yakoubi et al. (2016) have produced excellent quality CdZnS and Cu-doped CdZnS QDs through a facile and mild aqueous approach. The latter one, a highly emissive QD is made using novel capping agents like 3-mercaptopropionic acid (MPA) or N-acetylcysteine (NAC).

19.3.3 Biosynthesis

Biosynthesis or biomanufacturing is another promising route for the synthesis of metal sulfide QDs like CdS, ZnS, PbS, and Ag_2S (Prasad and Jha 2010) utilizing metal and sulfide ions as precursors and employing the intrinsic enzymatic machinery of microorganism. These ions using the magnesium or manganese transport system first enter into the cell cytoplasm and then get converted into nanocrystals by the intracellular enzymes located in the cytoplasm. Another route was developed known as extracellular synthesis where synthesis of QDs is caused by the enzymes occurring on the cell membrane or excreted to the medium. A single CdSe QD within yeast cells has been produced via genetic engineering of intracellular redox conditions. Further, it has been demonstrated that psychrotolerant, oxidative stress-resistant bacteria from Antarctic microorganisms are able to biosynthesize CdS QDs at low temperatures. Using an engineered strain of stenotrophomonas maltophilia (SMCD1), biosynthesis of CdS and PbS QDs was carried out reproducibly (Yang et al. 2016a). SMCD1 is capable of the direct extracellular biomineralization of CdS QD from a buffered aqueous solution of cadmium acetate and L-cysteine (Fig. 19.6) (Yang et al. 2016a).

In this route, L-cysteine performs both as a sulfur source and the capping agent. The optical properties of the QD can conveniently be controlled by varying the growth time. The progress of this low-temperature, aqueous phase synthesis route clearly indicates its superiority over chemical synthesis. This inherently green synthesis route has the potential to cut down production costs and lead to QDs with new/improved functionality (Yang et al. 2016a).

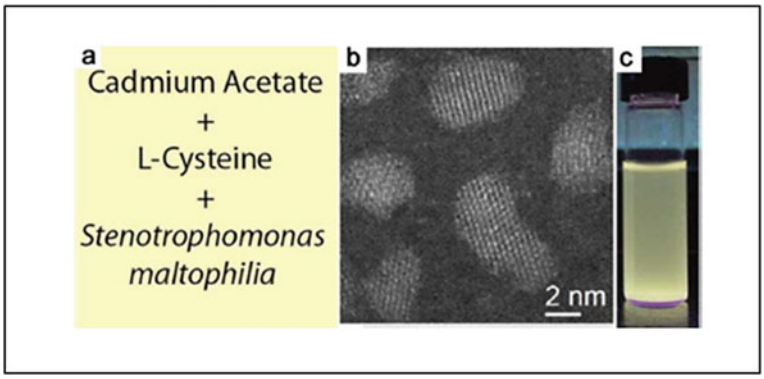

Fig. 19.6 **a** Components for biosynthesis of CdS QDs; **b** its high-resolution TEM image; **c** the visible fluorescence under UV illumination. Reproduced with permission from ACS Publications (Yang et al. 2016a)

19.4 Synthesis in Continuous Reactors

Typically, many reaction parameters were required to be controlled such as temperature, stirring rate, precursor injection position, and mixing to achieve good quality of the QDs. Gram-to-sub-kilogram quantities of QDs have been made in a single batch with proper process control. Recently, Bang et al. (2017) reported the single-batch gram-scale preparation of InP QDs using white phosphorus (P_4) as the precursor. However, in a traditional batch reactor, achieving proper control of the reaction parameters is challenging. To alleviate this, a continuous reactor concept is adopted where the reactants are fed continuously into the reactor and the product is continuously taken out. Since the parameters like temperature, pressure, and residence time are better controlled, a more consistent quality product is obtained.

19.4.1 Synthesis of QDs in Microfluidics

Microfluidic reactor has attracted attention as a promising technology for QDs synthesis since the first report in 2002 (Bang et al. 2010). Microfluidics are essentially continuous reactors integrated with heaters and fluid control elements. This arrangement provides much better control than in conventional macroscale batch-type reactors. Currently, such synthesis in microfluidic reactors is gaining much prominence.

Kikkeri and coworkers (2010) developed the microfluidics method to synthesize surface-functionalized CdSe and CdTe QDs (Fig. 19.7). The chemical reactions are similar to organometallic synthesis of QDs in batch reactors (Sect. 19.3.1). The most striking feature is its operation at a lower temperature (160 °C) than in a batch reactor

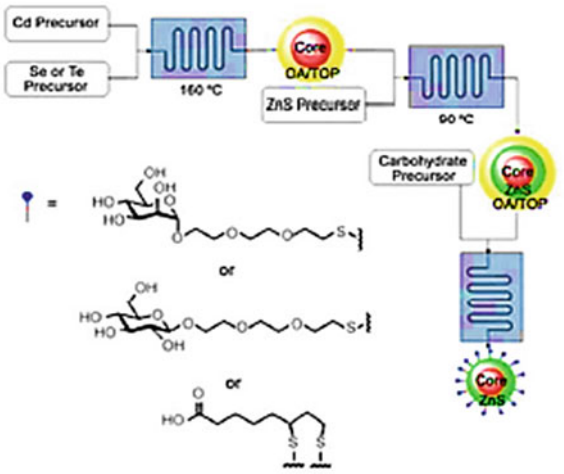

Fig. 19.7 Microfluidic reactor incorporating continuous-flow synthesis of functionalized QDs (OA: oleic acid; TOP: tri-n octylphosphine). Reproduced with permission from Wiley Publications (Kikkeri et al. 2010)

(~300 °C). Both CdSe/CdTe core and ZnS shell can be made in such continuous-flow microchannels. The sizes of the QDs can be tweaked by varying the reaction time in the reactor.

19.4.2 Thermospray Synthesis

This synthesis route requires organic ligands which get coated on the nanoparticles' surface preventing the agglomeration of QDs to make them highly dispersed in liquid solutions or solid composites. High-quality semiconductor QDs can be obtained by such spray-based method (Amirav et al. 2005). Using a thermospray nebulizer, aqueous or organic precursor solutions of semiconductor salts are first sprayed (Fig. 19.8) as monodispersed droplets. The precursor reaches over saturation as the droplets move forward and spontaneous condensation occurs due to the solvent evaporation. The ensuing QDs are free-standing, unsupported, and uncoated since each semiconductor dot is produced from a single spray droplet. Nanocrystals obtained using spray-based methods include the II–VI group like CdS, ZnS, and MnS, the IV–VI group PbS, and the metal sulfide such as MoS_2. Thermospray synthetic approach looks very attractive for all applications where films of uncapped and packed QDs are required.

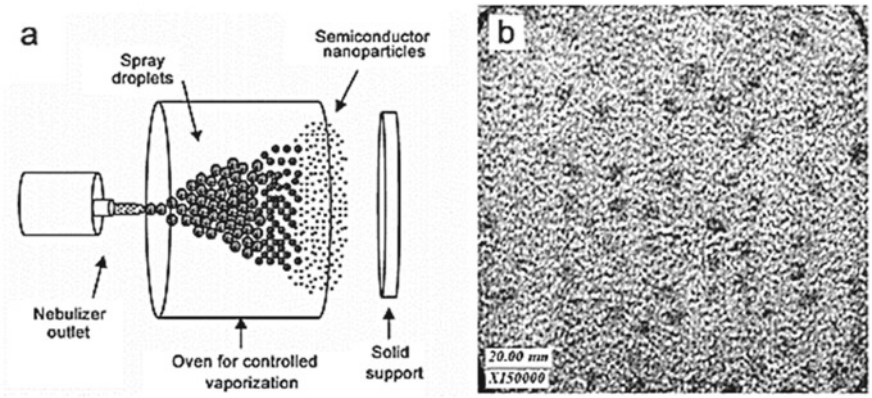

Fig. 19.8 **a** Production of CdS nanocrystals thermospray synthesis; **b** TEM image of CdS QDs (5.1 nm). Reproduced with permission from ACS Publications (Amirav et al. 2005)

19.5 Green Approach Using Electron Beam Irradiation

Radiation-assisted synthesis of nanomaterials is a very promising technique having several advantages: (a) simple, fast, and efficient method under moderate conditions, (b) commercial scale production, (c) since electron being a very strong reducing species ($E_{red} = -2.9$ V) does not require any external reducing agents, and (d) size controlling can be achieved by proper dose and irradiation time.

Sea urchin-like shaped CdSe nanoparticle is produced by this approach in aqueous solutions using citric acid (CA) as a capping agent. The sea urchin-like shaped nanocrystals being 3D in nature exhibit several novel properties, like good conductivity and a larger surface area and useful in several application areas of gas sensors, catalysis, and photovoltaics. Different shapes and sizes of the nanoparticles have been obtained depending on the types of templates or capping agents used during the growth (Liang-Shi et al. 2001). Elias et al. have reported the urchin-like nanostructures of ZnO, which holdgreat promise for photovoltaic applications (Elias et al. 2010). Moreover, compared with the 1D nanomaterials (i.e., nanorods, nanowires, nanotubes, and nanobelts), 3D ordered nanostructural materials can be regarded as the self-assembly of 1D nanomaterials, thereby increasing structural complexity and endowing the possibility of greater functions for some unique applications. Nonetheless, the concentrations of the individual precursors and the CA were optimized keeping in view the desired characteristics of the nanomaterials, i.e., colloidal stability, monodispersity, size tunability, and good PL properties. In the following sections, various techniques are presented which are normally used to characterize QDs. All these investigations along with the transient absorption studies performed by pulse radiolysis technique provided insight into the possible mechanism of such nanoparticle formation (Singh et al. 2013a).

19.5.1 Experimental Details

The precursor solutions were prepared with nanopure water. Sodium selenosulphate (Na_2SeSO_3), precursor for Se was made from 1 g Se powder, 10 g Na_2SO_3 in 50 ml nanopure water by refluxing the solution at 70 °C for 7 h. An appropriate amount of 25% ammonia was added to $CdSO_4$ solution, precursor for Cd till a clear ammoniated solution resulted. Subsequently, to this solution was added first freshly prepared Na_2SeSO_3 solution and then tertiary butanol. The capping agent CA was added to the reaction mixture just before the irradiation. This reaction mixture was irradiated with an electron beam from 7 meV linear electron accelerator (LINAC) at 12 pps rep rate delivering a dose of 140 Gy/pulse. Since the added tertiary butanol scavenged the radiolytically produced OH radicals, the coproduced e_{aq}^- interacts with the precursors inducing the synthetic reaction. The solution turned greenish-yellow or reddish-orange in color on irradiation, demonstrating the formation of the CdSe nanoparticles. The concentrations of CA and the precursor solutions were controlled appropriately to achieve the preferred morphology and the desired optical properties of the nanoparticles.

19.5.2 Pulse Radiolysis Technique

Elegant technique of pulse radiolysis was used to investigate the formation dynamics of the CdSe nanoparticles with a kinetic spectrometer. The aqueous solutions of both precursors containing equimolar (1 mM) amount mixed with 5 mM CA and 1 M tert-butanol. The transient species were monitored using white light from an Xe lamp (450 W) placed orthogonally to the electron beam. The dose measurement was carried out with a potassium thiocyanate, KSCN chemical dosimeter. The time-resolved kinetic traces of the generated intermediate species were recorded (Fig. 19.9) (Singh et al. 2013a).

N_2-purged solutions were used for all the experiments. Figure 19.9 exhibits two distinctive absorption peaks one at 380 nm (band-I) and the other at 510 nm (band-II). It may be noted that the band-I showed weaker absorbance compared to the band-II.

These observations corroborate well with the report of radiolytic formation dynamics in aqueous solution (Singh et al. 2011a). A plausible reaction mechanism for the synthesis of CdSe nanoparticles can be given:

$$e_{aq}^- + [Cd(NH_3)_4]^{2+} \rightarrow [Cd(NH_3)_4]^{\bullet +} \quad (k = 3.1 \times 10^{10}\, M^{-1}\, s^{-1})$$

$$e_{aq}^- + [SeSO_3]^{2-} \rightarrow [SO_3]^{2-} + Se^{\bullet -} \quad (k = 2.3 \times 10^{9}\, M^{-1}\, s^{-1})$$

$$[Cd(NH_3)_4]^{\bullet +} + Se^{\bullet -} \rightarrow (CdSe)_{solvated} \rightarrow (CdSe)_{np}$$

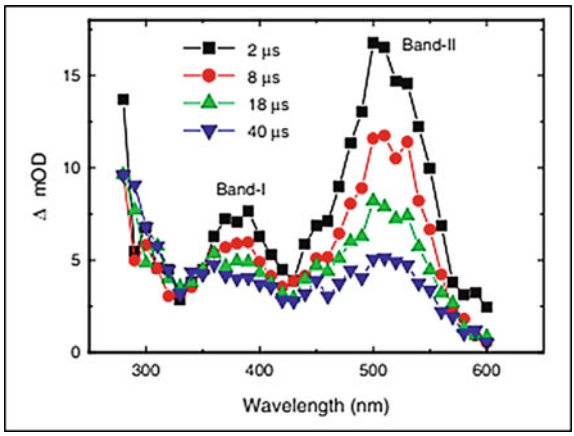

Fig. 19.9 The time-resolved kinetic traces of the generated intermediate species: [precursor] = 1 mM; [CA] = 5 mM and absorbed dose = 25 kGy. Reproduced from American Scientific Publishers as author of this work (Singh et al. 2013a)

The CA molecules facilitate in attaining a sea urchin-like structure by chelating the primary nanoparticles formed which could be due to their tridentate capping nature and short chain length. It may be noted that during the production of nanoparticles, many complex transient species are also generated similar to those reported in Singh et al. (2011a):

$$\left[Cd(NH_3)_4\right]^{2+} : Se^{\bullet -};\ \left[Cd(NH_3)_4\right]^{\bullet +} : [SeSO_3]^{2-};\ \text{and}\ \left[Cd(NH_3)_4\right]^{\bullet +} : Se^{\bullet -}$$

19.6 Characterization of QD

19.6.1 Optical Absorption

The unirradiated solutions containing precursors (1 mM each of Cd and Se precursor) and CA (5 mM) did not show any absorption in the 350–700 nm region (Fig. 19.10). However, the solutions on irradiation showed a clear excitonic peak at around 420 nm. This result confirms that the formation of CdSe nanoparticles takes place by electron beam irradiation. Three important parameters, namely, absorbed dose, precursors' concentrations, and the capping agent, CA were optimized. The solutions irradiated at an absorbed dose of 25 kGy (containing 5 mM CA) changed color from pale yellow to dark orange, as the precursors' concentrations were increased from 1 to 10 mM. These changes are clearly visible in the camera-ready pictures as shown in the top panel (I) of Fig. 19.11 (Singh et al. 2013a).

It may be mentioned that aqueous synthesis of CdSe nanoparticles using equimolar ammoniated $CdSO_4$ and Na_2SeSO_3 solutions, through electron beam irradiation, has been previously reported (Singh et al. 2011b). Therefore, the present investigation expected to produce CdSe nanoparticles was confirmed by XRD measurements. CA

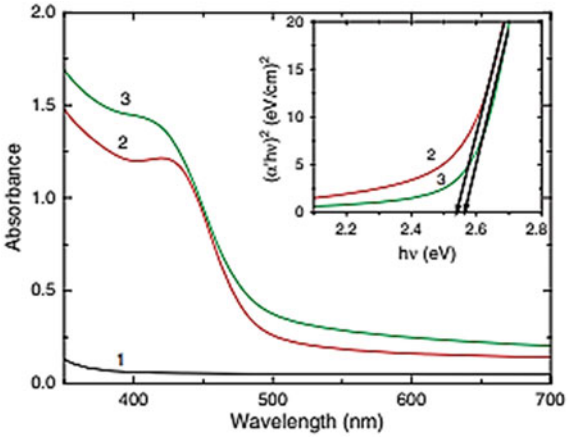

Fig. 19.10 Absorption spectra of unirradiated (1) and irradiated (2, 3) reaction mixtures (25 kGy) containing different equimolar precursor concentrations with a fixed concentration of CA, 5 mM. Precursor concentrations in mM: (1) 0.5 (2) 0.5 (3) 1.0. Inset: Tauc plot of $(\alpha' h\upsilon)^2$ versus $h\upsilon$ for band gap (E_g) determination. Reproduced from American Scientific Publishers as author of this work (Singh et al. 2013a)

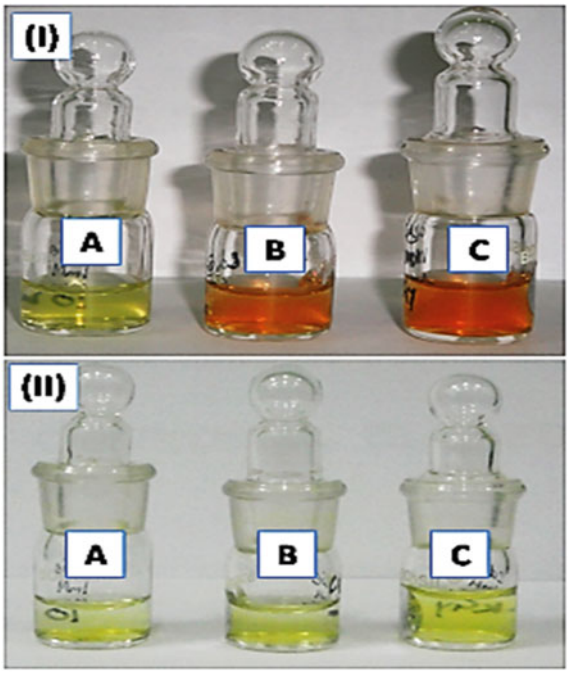

Fig. 19.11 Camera-ready pictures of CdSe prepared by electron beam irradiation. **I** Absorbed dose is kept constant at 25 kGy, [precursors] in mM: (A) 1 (B) 5 (C) 10; **II** fixed [precursors] = 1 mM, fixed [CA] = 5 mM, absorbed doses in kGy: (A) 10 (B) 25 (C) 40. Reproduced from American Scientific Publishers as author of this work (Singh et al. 2013a)

is also known to be a good reducing agent ($E = -1.1$ V vs. Ag/AgCl) and therefore its concentration was optimized in order to avoid any chemical reduction process. It was further observed that the CdSe particles precipitate at a concentration of precursors higher than that of CA, which could be due to the fact that the available concentration of the capping agent was not able to cap the as-grown CdSe nanoparticles efficiently. Therefore, the concentration of the precursors was optimized at 1 mM, where the nanoparticles do not settle down through further agglomeration. Besides, it was noticed that CA with a concentration $\leq$5 mM, produces well-separated smaller spherical nanoparticles. Further, a higher concentration of CA could lead to destabilization effect and induce coalescence, hence was avoided in this study. From these observations, optimized concentrations of precursors and CA were found to be 1 and 5 mM, respectively.

Using the absorption spectra and modified Brus equation the primary CdSe nanoparticles' sizes were calculated and are listed in Table 19.1

$$E_g = E_g(0) + \alpha/d^2$$

where $\alpha = 3.7$ eV nm^2, $E_g(0) = 1.75$ eV, d = particle size in nm, and E_g = band gap in eV. Since this is a direct band gap semiconductor the band gap values were determined from the Tauc plot of $(\alpha' h\upsilon)^2$ versus $h\upsilon$ (inset of Fig. 19.10). The symbol "α" represents the absorption coefficient multiplied with the concentration of the CdSe nanoparticles, calculated from the relation (2.303 A/l), where "A" is the absorbance and "l" represents the cell length (10 cm) and the term "$h\upsilon$" is the photon energy. The estimated values of the particle sizes were between 2.07 and 2.70 nm.

The dependence of absorbed dose on the particle formation was investigated under optimized concentrations of CA and precursors. The camera-ready pictures (showing the dose effect) of the irradiated sol containing the CdSe nanoparticles are shown in the bottom panel (II) in Fig. 19.11. A pale yellow color of the sols with no difference in all three cases is apparent. However, from Fig. 19.10, it is evident that the absorbance increases with the increase of dose (10–25 kGy) and then starts decreasing up to 40 kGy. This was associated with a slight red shift in the excitonic peak position. Correspondingly the particle size increased from 2 to

Table 19.1 Optical absorption measurements yield the CdSe band gap (eV) and nanoparticle size (nm) synthesized with electron beam irradiation (Singh et al. 2013a)

Absorbed dose (kGy)	[Precursor] (mM)	[CA] (mM)	E_g (eV)	Particle size (nm)
25	0.5	5	2.54	2.08
25	1.0	5	2.56	2.07
25	5.0	5	2.25	2.59
25	10.0	5	2.20	2.70
10	1.0	5	2.62	2.00
25	1.0	5	2.56	2.07
40	1.0	5	2.45	2.22

2.22 nm. Instantaneous agglomeration of the particles was observed when the dose exceeded 25 kGy possibly due to radiolytic degradation of CA. Therefore, under the present experimental conditions, 25 kGy seemed to be the optimum dose for the precursors' concentrations of 1 and 5 mM for CA.

19.6.2 TEM, SEM, and XRD

Various characterization techniques TEM, SEM, and XRD were applied for CdSe nanoparticles. The TEM images (Fig. 19.12a) indicated an agglomerated form of CdSe nanoparticles of size about 500 nm, closely resembling sea urchin-like shapes (Singh et al. 2013a). However, the primary nanoparticles were within 3 nm in size. These values were in well agreement with those obtained from the absorption studies. The small angle electron diffraction (SAED) patterns of these nanoparticles show their amorphous nature. The SEM images shown in Fig. 19.12b, also confirm the existence of particles with sea urchin-like shapes and these agglomerates consisted of smaller units of identical patterns (Singh et al. 2013a).

Miller indices for the diffraction patterns are marked in the figure (Fig. 19.13a) and are attributable to those of CdSe (JCPDS Card No. 19-0191) (Singh et al. 2013a). The broadening in the peaks specifies the amorphous nature of synthesized CdSe nanoparticles. The growth process is restricted by the capping agent, CA and so, smaller size (<3 nm) CdSe nanoparticles could be obtained by electron beam irradiation method. However, the primary CdSe nanoparticles being ultra-small and amorphous in nature possess high surface energy, and therefore undergo oriented aggregation of nanoparticle subunits assisted by the CA molecules. In fact, CA is a tridentate chelating ligand having three carboxylic groups and one hydroxyl group, thereby expectedly acting as a structure-directing molecular-coordination stabilizer. Consequently, the

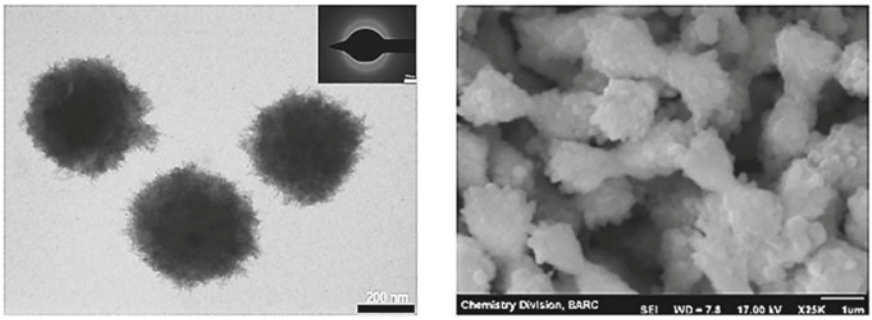

(a) **(b)**

Fig. 19.12 **a** TEM and **b** SEM image of synthesized CdSe nanoparticles with electron beam irradiation. The parameters are: [precursor] = 1 mM, [CA] = 5 mM; absorbed dose = 25 kGy. Reproduced from American Scientific Publishers as author of this work (Singh et al. 2013a)

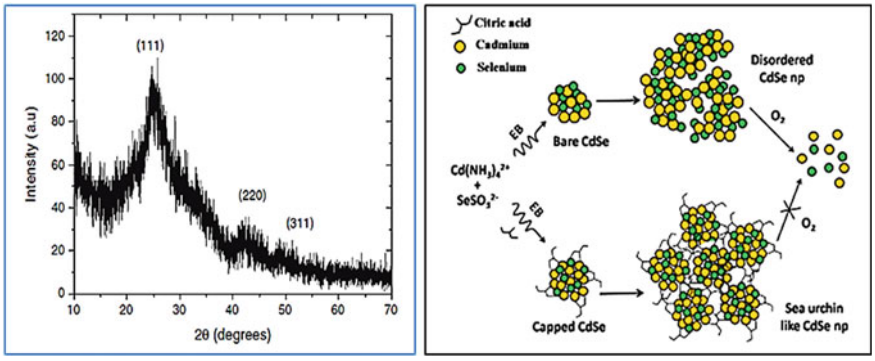

Fig. 19.13 **a** Room temperature XRD pattern of as-grown CdSe nanoparticles. **b** Scheme 1 showing different growth patterns upon EB irradiation in the presence and the absence of capping agent (CA). Reproduced from American Scientific Publishers as author of this work (Singh et al. 2013a)

chelating ability of this molecule for the initially formed amorphous nanoparticles is most likely leading to a 3D anisotropic morphology closely resembling that of sea urchins (Fig. 19.13b; Scheme 1). Basically, seeded growth process along with the kinetically driven mechanism lead to the anisotropic shapes of the nanoparticles. Thus, the phenomenon can be described on the basis of the interaction between the stochastic diffusive forces arising out of nucleation and growth of initially formed primary CdSe nanoparticles into spherical aggregates. They subsequently re-orient into the radially expanding sea urchin-like shapes (see Scheme 1), under the directive forces of CA molecules.

This is further corroborated by the mechanism proposed by Kamat (2008) where it had been shown that initially a few seeds of CdSe nanoparticles are formed, which strongly complex with the citrate anions. It reaches an optimal size by gradual growth of the agglomerates and after reaching that stage further aggregation is prevented by the strong repelling layer of citrate. Subsequently, the Ostwald ripening process produces larger particles. However, in the absence of capping agents, the bare CdSe nanoparticles do not exhibit any preferred morphology, rather settled in disordered agglomerated structures. The uncapped CdSe nanoparticles were found to be unstable upon exposure to air/oxygen (see Fig. 19.13b; Scheme 1), while the capped nanoparticles synthesized in the above studies were found to be quite stable. Therefore, it is recognized that the CA molecules help in achieving the stabilized sea urchin-like shaped nanoparticles and prevent them from reacting with oxygen unlike that observed in the case of bare CdSe nanoparticles (Singh et al. 2010).

19.6.3 Photoluminescence (PL)

The emission spectra of the freshly prepared as-grown CdSe nanoparticles clearly showed 520 nm band gap photoluminescence (BG-PL) and 600 nm trap state photoluminescence (TS-PL), and was found to be independent of the excitation wavelengths at room temperature. The trap states are probably due to unsaturated surfaces involving dangling bonds arising from high dose rate encountered in this synthesis process (Singh et al. 2010). CA is also capable of altering the surface properties thereby reducing the surface defects, which result in obtaining BG-PL in these nanoparticles. However, the uncapped nanoparticles synthesized in aqueous solutions containing similar precursors do not exhibit any PL (Singh et al. 2011b). Interestingly, the CdSe nanoparticles formed in cetyl trimethyl ammonium bromide (CTAB) based water-in-oil microemulsions via electron beam irradiation exhibit strong TS-PL at room temperature (Singh et al. 2013b). However, the CdSe nanoparticles formed through a similar synthesis route in the present study exhibit both BG-PL as well as TS-PL. This demonstrates that CA plays a dual role in stabilizing these nanoparticles under ambient conditions and enhancing the radiative decay pathways for the photoexcited carriers in these nanoparticles.

Using the TCSPC instrument, the time-resolved PL measurements were carried out at room temperature, the excitation and the emission wavelengths, respectively, being 445 and 580 nm (Fig. 19.14).

Assuming tri-exponential decay, the profile was best fitted with the parameters shown (in red) in the figure. The weighted average lifetime was estimated to be 350 ps. The short lifetime component may be due to the BG-PL, whereas the other

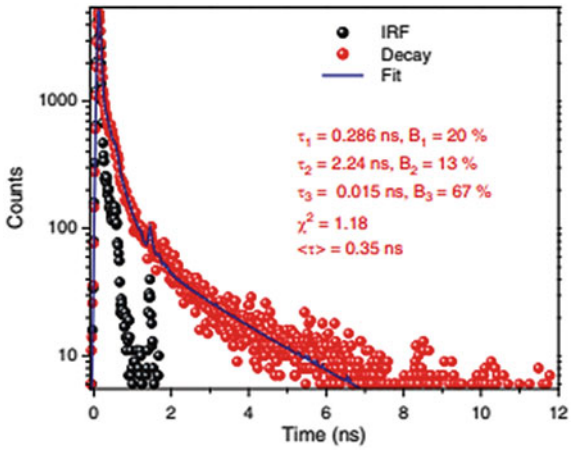

Fig. 19.14 Lifetime emission decay curve (red dots) and IRF (black dots) and the best fitted curve for electron beam synthesized CdSe nanoparticles. The parameters are: [precursor] = 1 mM, [CA] = 5 mM, dose = 25 kGy; and λ_{exc} = 445 nm, λ_{emi} = 580 nm. Reproduced from American Scientific Publishers as author of this work (Singh et al. 2013a)

two arise from the trap states. The decay pattern indicates the existence of different deep and shallow trap states in these nanoparticles. A similar trend of PL lifetime values was seen in case of synthesis in CTAB-based water-in-oil microemulsions (Singh et al. 2013b), but the contribution from the BG-PL was quite less compared to the present case. The weighted average lifetime is found substantially longer (4.1 ns) and possibly due to the variance in the surface structure in these two cases.

19.6.4 Raman Spectroscopy

Raman spectroscopy reveals the composition, crystal quality w.r.t. orientation, symmetry, and lattice stress/strain effects of II–VI semiconducting nanomaterials. Room temperature Raman spectra of as-grown CdSe nanoparticles capped with CA (Fig. 19.15) comprises of fundamental longitudinal optical (LO) phonon peak at 206.9 cm^{-1} and its overtone (2LO) peak at 411 cm^{-1}, respectively. An additional shoulder indicating transverse optical (TO) phonon mode is shown near 168 cm^{-1} (Mauro et al. 2008). In addition, the spectrum contains background, which reveals the luminescent nature of as-grown nanoparticles.

A weak wide peak at ~250 cm^{-1} seen in the Raman spectra is due to the small size (2–3 nm, Table 19.1) of these nanoparticles along with their amorphous nature (from XRD spectra and SAED pattern). The appearance of the surface optic (SO) modes near 250 cm^{-1} can be attributed to the extra atoms present on the surface compared to the bulk. There is a red shift observed for LO peak of CdSe nanoparticles from its bulk position at 210–213 cm^{-1}. The size reduction is mostly controlled by quantum confinement but dimensional effects like surface reconstruction and lattice contraction also play some role.

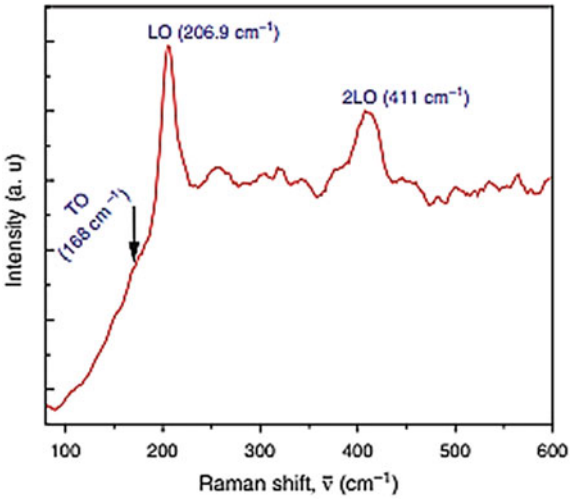

Fig. 19.15 Raman Spectra of electron beam synthesized CdSe nanoparticles. The parameters are: [precursor] = 1 mM, [CA] = 5 mM, and absorbed dose = 25 kGy. Reproduced from American Scientific Publishers as author of this work (Singh et al. 2013a)

The reduced dimensions bring about competition between confinement and strain effects. Consequently, LO peaks experience red shift with respect to their bulk when phonon confinement or strain effect occurs. However, the present observed red shift is due to the phonon confinement effect because the primary nanoparticles (between 2 and 3 nm; Table 19.1) reasonably smaller than the Bohr exciton radius of CdSe (5.6 nm). Further, the LO peak asymmetry with its broadening is sign of the phonon confinement and the structural disorder on the surface. This structural disorder responsible for the rise of surface defects, is corroborated from the broad PL spectra of as-grown CdSe nanoparticles. However, XRD analysis indicated tensile stress leading to lattice contraction. The lattice constant value, "*a*" was found to be 5.97 Å, which is slightly lower than cubic CdSe (6.07 Å). The reason for this lattice contraction is probably due to the surface tension-induced reconstruction on the surface. In effect, the red shift in the LO peak relative to the bulk appears to be the combined result of the phonon confinement and tensile stress. However, the former effect seems to have the dominant role in the observed shift.

19.7 Shape Evolution of Nanomaterials in Microheterogeneous Media

Since QDs' shape is crucial in deciding newer material properties, synthesis of CdSe nanomaterials is investigated in microheterogeneous media (i.e., water-in-oil type microemulsions) using the surfactant, cetyl trimethyl ammonium bromide (CTAB) and cyclohexane as the oil. The central interest is to examine whether the shape evolution of the QDs in such a medium is different compared to an aqueous solution. The investigations were carried out under two different experimental conditions (Singh et al. 2013c): (i) by normal chemical route at room temperature and (ii) by 7 meV electron beam irradiation route. In both the routes, CdSe nanomaterials were produced first in isotropic spherical shape and then evolved to anisotropic rod-like structures. However, the photoluminescence of the CdSe nanomaterials was found to be remarkably different in two cases. In the chemical route, initially, the band gap photoluminescence was observed which changed with aging. After a day, two distinct BG-PL along with TS-PL were recorded. On the other hand, radiation chemical synthesis provided dominant trap state photoluminescence (TS-PL), which persisted even after aging.

In-depth mechanistic investigation on the electron beam synthesis of CdSe nanomaterials was carried out in water-in-oil type microemulsions with less water content, ($w_0 < 20$). It is well established that water undergoes radiolysis and yields three major primary radial species, out of which e_{aq}^- and H are reducing and OH is oxidizing in nature (Spinks and Woods 1976). Tert-butanol (CH_3 $(CH_3)_2COH$) added in the aqueous solution leaves behind hydrated electrons, e_{aq}^- after scavenging the OH/H radicals. This can be termed as a perfectly reducing condition where the reduction is

done through the e_{aq}^- species. This reduction of precursor ions produced CdSe nanomaterials (Singh et al. 2011a). Thus, under the above conditions, the steps involved are similar to that described in Sect. 19.5.2:

Radiolysis of water:

$$H_2O \rightsquigarrow e_{aq}^-,\ OH^{\bullet},\ H^{\bullet},\ H_3O^+,\ H_2,\ H_2O_2$$

Followed by

$$OH\bullet\ (H\bullet) + CH_3(CH_3)_2COH \rightarrow \bullet CH_2(CH_3)_2COH + H_2O\ (H_2)$$

$$e_{aq}^- + \left[Cd\ (NH_3)_4\right]^{2+} \rightarrow \left[Cd\ (NH_3)_4\right]^{\bullet +}$$

$$e_{aq}^- + [SeSO_3]^{2-} \rightarrow [SO_3]^{2-} + Se^{\bullet -}$$

$$Cd^{\bullet +} + [SeSO_3]^{2-} / Se^{\bullet -} \rightarrow (CdSe)_{intermediate} \rightarrow (CdSe)_{np}$$

The radiolytic synthesis turns the colorless microemulsion into a greenish-yellow color. The TEM image of the as-grown CdSe sols showed isotropic spherical nanoparticles (<5 nm) which agglomerated to relatively bigger sizes. The optical absorption spectra showed an intense 450 nm peak. However, the TEM image of the sol recorded after a day's aging, confirmed the rod-shaped CdSe nanomaterials and its absorption peak showed a slight red shift as seen in Fig. 19.16a. It can be seen that the room temperature PL peak at 600 nm (TS-PL) dominates over the hump at 525 nm (BG-PL) (Fig. 19.16b), which gets further augmented with aging. As already shown, this observation was quite different from the result of the chemical route. This is possibly due to the combined effect of internal structure and the defect sites. It is known from the literature that radiation-induced synthesis normally produces nanomaterials with disordered structures with low crystallinity and higher defect density (Singh et al. 2010, 2011b; Kamat 2008). Therefore, the observed photoluminescence behavior may be ascribed to the above factors.

19.8 Shape Evolution in Room Temperature Ionic Liquids (RTIL)

Room temperature ionic liquids (RTIL) have many distinctive properties like very low vapor pressure, good ionic conductivity, large polarity, and stability. These class of compounds have recently been used as media for the nanomaterials synthesis. Though a couple of reviews have already appeared in the literature (Ma et al. 2010), the literature is sparse regarding the role of in-built structure of IL in regulating

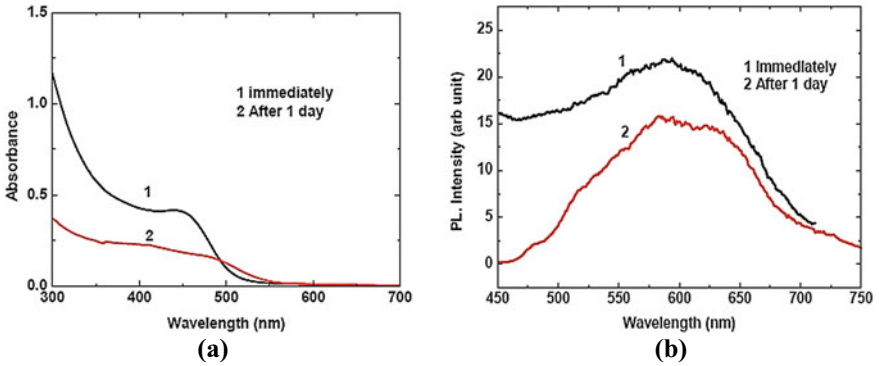

Fig. 19.16 **a** Optical absorption spectra **b** photoluminescence spectra of electron beam synthesized CdSe nanoparticles in water-in-oil type microemulsions with water content ($w_0 = 10$); [precursor] = 10 mM; spectra recorded at different times to check the stability. It is reproduced from the International Association of Advanced Materials as author of this work and under Creative Common License (Singh et al. 2013c)

the nanoparticles' growth and morphology. For a better understanding in this area, the synthesis of CdSe nanoparticles is investigated in a well-studied IL, 1-ethyl-3-methyl imidazolium ethyl sulfate ([EMIM][EtSO4]). The RTIL played three roles in the synthesis such as (i) solvent, (ii) stabilizer, and (iii) shape directing template. The primary nanoparticles produced (2–5 nm range) were characterized by HR-TEM. Then these nanoparticles evolve as nano flake-like units. They further self-assemble and appear as a mixture of 2D sheets and 3D flower-like patterns as revealed by the SEM technique. The stability of these coexisting nano morphologies identifies the inherent microheterogeneity of the RTIL (Guleria et al. 2014).

Figure 19.17 represents the TEM images of the as-grown nanoparticles (Guleria et al. 2014) while its polydispersity (2–5 nm range; average size ~2 nm) is shown in Fig. 19.17b representing the HRTEM image. The most interesting aspect revealed is the self-assembling into some type of superstructures (Fig. 19.17a). Self-assembling was further probed with SEM recorded at different regions (Fig. 19.18) (Guleria et al. 2014). In the inset of Fig. 19.18a, the energy-dispersive X-ray analyzer (EDX) spectrum confirmed the formation of nanoparticles. One unusual peak indicating Si is possibly due to the Si-wafer substrate used in the analysis. Figure 19.18a indicated the globular shape of the primary nanoparticles which later evolve as nano flake-like (NF) structures (arrows in Fig. 19.18b). Later, the formation of a mixture of 2D nanosheets and 3D nanoflower structures from self-assembling of NFs is presented in Fig. 19.18c, d. It is to be noted that the morphologies were quite stable over a long time period. This is indicative of the excellent stabilizing effect of RTIL in preserving the nano morphologies.

SEM images reveal that due to the high surface area of the NFs, they assemble non-homogeneously to form 2D and 3D nano or even micro-organizations. The multilayered 2D sheet structures (10–15 μm long and 1–2 μm wide) (marked in

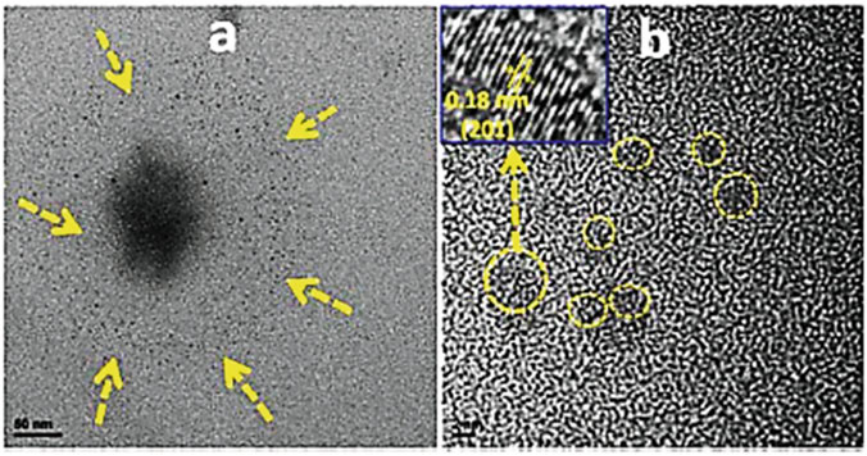

Fig. 19.17 **a** TEM (50 nm scale) and **b** HRTEM image (2 nm scale) of the CdSe nanoparticles made in neat RTIL. The inset of (**b**) presents the lattice fringe pattern (0.18 nm interplanar distance, plane 201) of the CdSe hexagonal phase. Reproduced with permission from RSC Publications as author of this (Guleria et al. 2014)

Fig. 19.18d) originate from the fusion of NFs. It may be worth mentioning that this field is growing at a rapid rate where recent syntheses assisted by RTILs are reported for ZnS nanoparticles, flower-like MoS_2, PbS nanocubes, and CdSe hierarchical dendrites.

Furthermore, FT-IR and Raman spectroscopic investigations indicate $\pi-\pi$ stacked aromatic geometry and the hydrogen bond network between the nanoparticles and RTIL cation/anion. Few control experiments were carried out in dilute RTIL with varying water content. The morphology was examined as a function of water content and time. A probable mechanistic scheme is shown in Fig. 19.19 (Guleria et al. 2014) depicting the formation and evolution of the whole series of events employing the RTIL structure and its fluidic aspects.

19.9 Core–Shell Quantum Dots

Two major factors, quantum confinement and surface effects, as discussed in earlier sections influence the QDs' properties. These effects are realized in the development of optoelectronic devices and medical applications. Many basic bulk material properties like melting point, solubility, reactivity, plasticity, magnetism and conductivity, etc., get transformed when QDs are formed. These QDs get easily dispersed in solvents and can be functionalized at their surface. It may be stated again that capping the surface is vital for obtaining luminescent and stable QDs. There are two

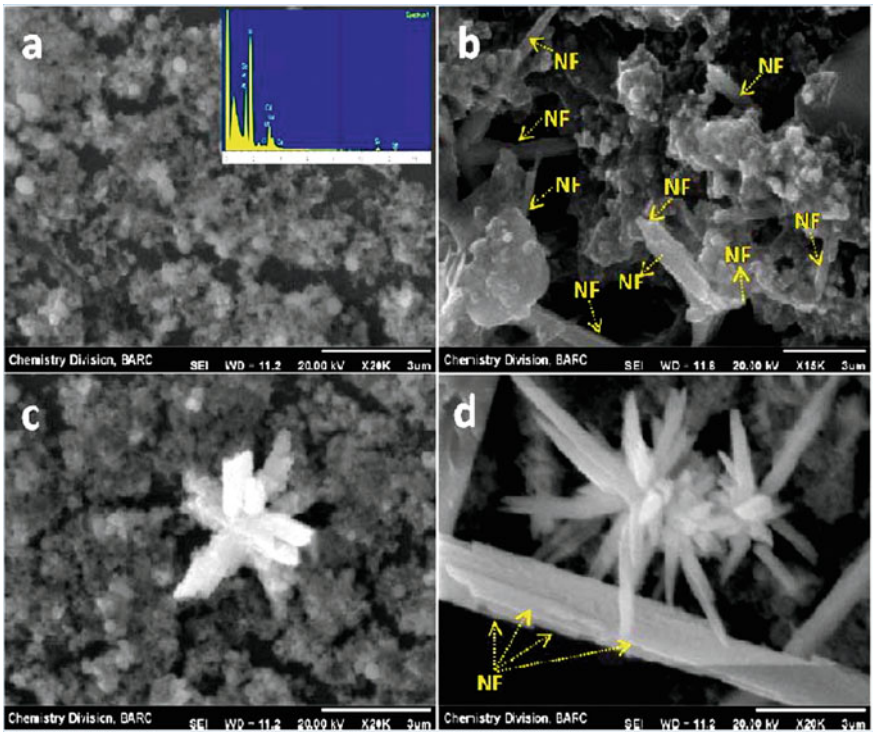

Fig. 19.18 The different transient stages of as-grown CdSe nanostructures recorded with SEM after 5 h of the reaction. They are **a** globular shape **b** NF structure **c** 3D flower-like pattern and **d** 2D nanosheet-like structures (scale bar is 3 μm for (**a**)–(**d**)). Reproduced with permission from RSC Publications as author of this (Guleria et al. 2014)

ways of achieving such capping (i) organic route and (ii) inorganic route (Fig. 19.20) (Bera et al. 2010).

Capping action of organic molecules is provided by binding with surface atoms. The benefits of the above passivation result in monodispersity, colloidal suspension, and bio-conjugation. However, because of large organic capping molecular size, it is not always possible to passivate cation and anion surface sites and achieve full coverage of the surface. But the other strategy namely the inorganic passivation can fully passivate surface trap states by growing another semiconductor layer over the QD. In subsequent sections, the resultant substance called core–shell QDs (CSQD) will be dealt with in detail. In such CSQD, fluorescence QY and photostability are considerably improved. By selecting suitable core and shell materials and their dimensions, the absorption and emission spectra, and other desirable properties can be controlled. However, if there is a considerable mismatch of core and shell lattice structures, the resulting lattice strain produces defect sites. The thicker shell also generates misfit dislocations, which increase the non-radiative processes further and decrease the fluorescence QY.

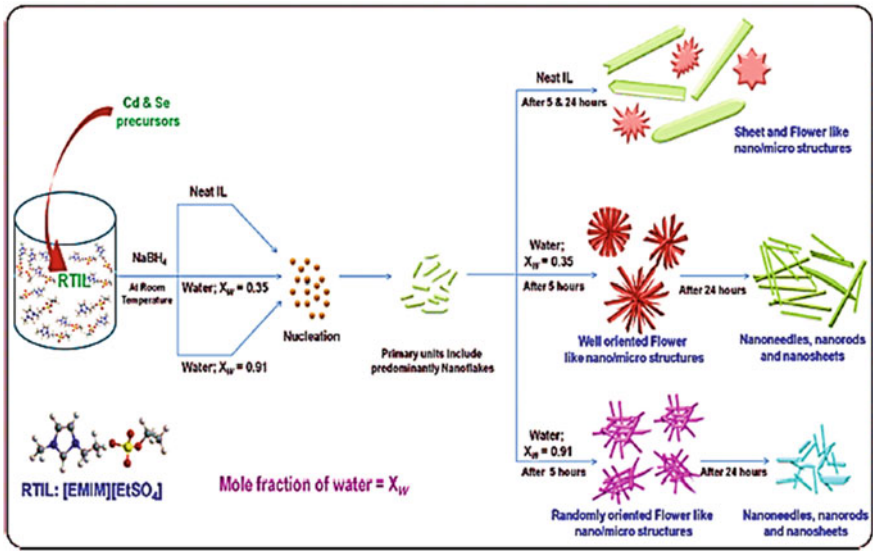

Fig. 19.19 Mechanistic scheme depicting the formation and evolution of the whole series of events in RTIL, ([EMIM][$EtSO_4$]), as a function of time and mole fractions of water. Reproduced with permission from RSC Publications as author of this (Guleria et al. 2014)

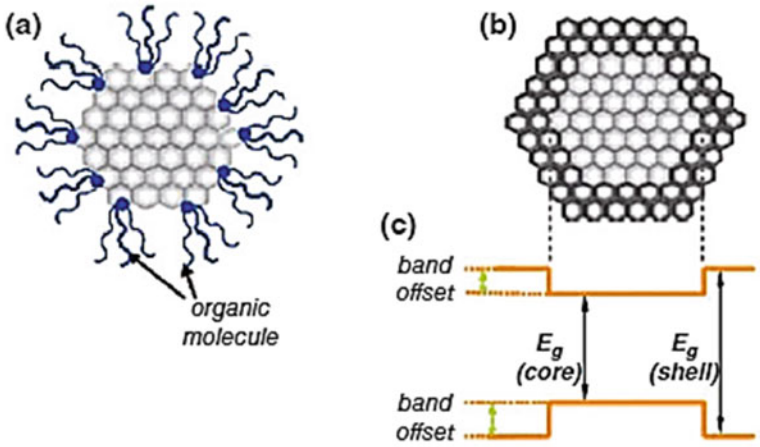

Fig. 19.20 Passivation of QD **a** organic way **b** core–shell QD by inorganic way and **c** energy band offsets of CSQD. Reproduced from MDPI Publications under Creative Common Licenses (Bera et al. 2010)

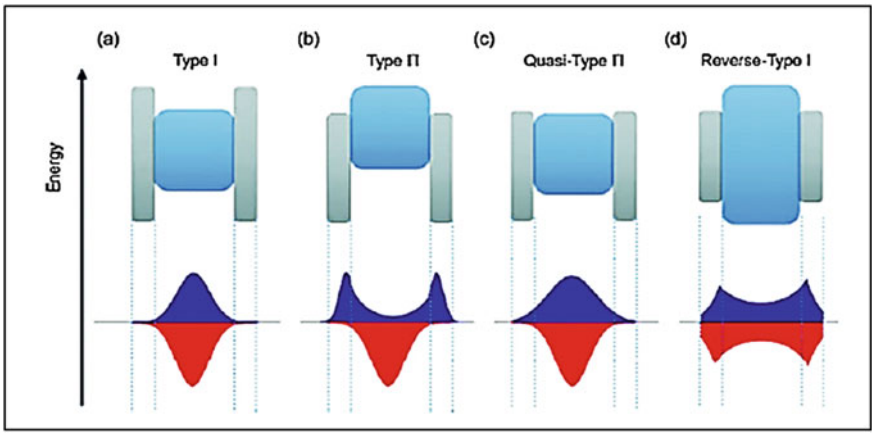

Fig. 19.21 **a** Type I, **b** type II, **c** quasi-type II, and **d** reverse type I CSQD materials: and their band alignment. Electron wave function is denoted by blue and the hole wave function by red color. Reprinted with permission from RSC publications (Zhou et al. 2018)

19.9.1 Classification of Core–Shell Quantum Dots

Three categories of CSQDs, namely, type I, reverse type I, and type II are obtainable depending on the energy bandgap offset (Fig. 19.21). Type I material is represented conveniently where $E_{g,\text{shell}} > E_{g,\text{core}}$ and the charge carriers are enforced within the core. In reverse type I material, the above bandgaps are in reverse order and the charge carriers get partially or completely delocalized within the shell. Finally, in type II, either valance or conduction band edge of shell material lies inside the bandgap of the core material. Consequently, upon photoexcitation, the charge carriers are spatially quarantined in a ditinct region of core–shell heterostructure (Reiss et al. 2009; Zhou et al. 2018).

Additionally, there is an intermediate type of core–shell structure, termed quasi-type II core–shell QDs. The most considered in this category is CdSe/CdS CSQD, although essentially, it is a type I structure. Here the electronic wave function gets delocalized over the entire nanocrystal, while the core material contains the hole wave function (Reiss et al. 2009; Zhou et al. 2018).

19.9.2 Type-I Core–Shell Structures

The major transformation of semiconductor QD is the strongly enhanced band gap fluorescence compared to the bulk phase. When all surface valences are satisfied during synthesis, the surface is termed as well-passivated and QY gets enhanced drastically. In the case of weakly bound capping agents, a dynamic equilibrium of adsorption/desorption results, and they are also sensitive to post-synthetic treatments.

Thus robust method of passivating the surface is needed to produce stable QDs with pronounced quantum yields.

Innovative investigations were conducted where a significant enhancement of QY of CdS QDs obtained by treating with hydroxide ion in the presence of excess Cd^{2+}. A passivating $Cd(OH)_2$ shell formed around the QD prevents the movement of free charge carriers to surface trap states.

Most of the CSQDs are synthesized in high-boiling organic solvents following the procedure of Murray et al. (1993). This organic solvent synthesis provides less polydisperse material compared to the aqueous synthesis route. The first successful shell made of ZnS over CdSe QDs was achieved in 1996 by Hines and Guyot-Sionnest (1996) followed by further work on CdS/CdSe QDs.

The above two CSQDs with high fluorescence QY have been investigated in detail, and are treated as "hydrogen atom" for QDs. Standard core material, CdSe (band gap of 1.7 eV; 728 nm), is chosen for using the entire visible radiation with 1.7–6 nm QD size. Based on two different reasons ZnS and CdS are commonly used as shell materials on CdSe core. Since ZnS has a large band gap (3.7 eV), it is possible to confine the free charge carriers in the core even with a thin shell configuration. But its synthesis via epitaxial growth route is rather difficult due to lattice mismatch in CdSe–ZnS. However, CdS over CdSe offers relatively low lattice mismatch, even with moderately thick shells. But its smaller band gap (2.5 eV) compared to ZnS, leads to less effective electronic passivation for a certain shell thickness.

Figure 19.22 represents the absorption and emission spectra of CdSe/CdS CSQD. Two key inferences can be drawn from the above spectra: (i) with increasing shell thickness, the first absorption maximum gets red-shifted and (ii) the QY of the core–shell configuration is higher compared to the bare QD. These are due to both the charge carriers' relaxation into the CdS shell, while the QY increase is due to surface trap state passivation. For ZnS shell, the observations are similar but the red shift of the absorption maximum is less prominent. It may be noted that the QY reaches a maximum with 1.8 monolayers thick ZnS shell. Such maximum in QY happens due to considerable lattice mismatch. Subsequently, extensive works have been carried out to achieve simple control of the shell thickness for making better devices. Presently, other than the above two, a large variation of type-I CSQDs have been prepared (Hines and Guyot-Sionnest 1996; Li et al. 2003), which include CdS/ZnS, and InP/ZnS.

It may be noted that due to their significant photo and chemical stabilities plus high QY, type-I CSQDs are fast replacing the organic dye molecules in bio-labeling. This kind of in-vitro or in-vivo biolabeling is quite useful in detecting/monitoring the photoluminescence (PL) of the QD (cf. Sect. 19.11.6). In particular, the greatly enhanced photostability along with narrower emission line width compared to the organic dyes, make these CSQDs prospective candidates for even multicolor labeling.

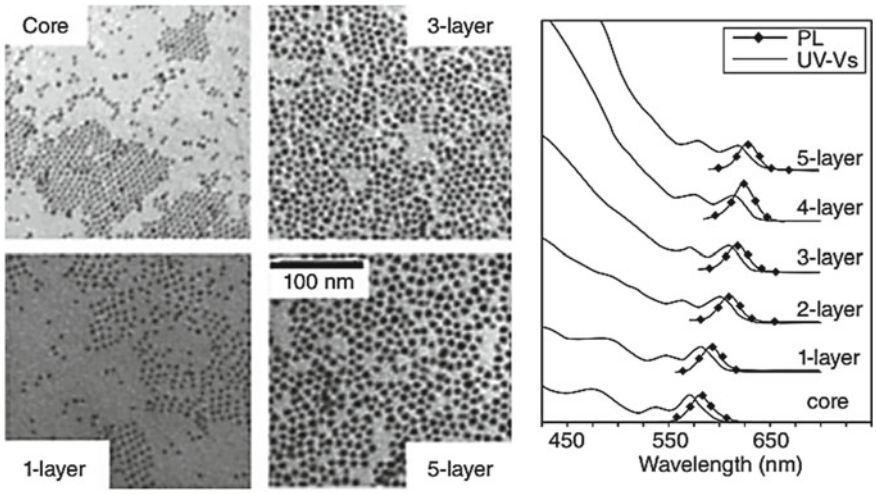

Fig. 19.22 Left: TEM images of bare CdSe and CSQD with CdS shell of 1, 3, and 5 monolayers thick; right: spectra (absorption and emission) of all the configurations. Reprinted with permission from ACS publications (Li et al. 2003)

19.9.3 Type-II Core–Shell Structures

It has been discussed (Sect. 19.9.1) that characteristics of type II core–shell structures arise due to the shell material's valance or conduction band edge lying inside the core material's bandgap. Therefore, the charge carriers produced on photoexcitation are spatially restrained in distinctive regions of the core–shell heterostructure (Hines and Guyot-Sionnest 1996; Li et al. 2003). In effect, the electron and hole being in two different locations undergo remarkably slower recombination rate prolonging the luminescence lifetime.

Usually, type-I nano heterostructures have better performance than core QDs in regard to their fluorescence QY and photostability. But, type-II heterostructures behave differently compared to type-I or core QD material. In this case, due to staggered band alignment, spatially indirect transition occurs at energies lower than both core and shell materials' band gaps. Therefore, the emission of type-II materials occurs at different wavelengths than either type-I or core QDs. Moreover, the luminescence lifetime of type-II heterostructures is observed to be shorter than type-I material.

A promising application of type-II materials namely QD laser has recently been demonstrated. The band alignment and slight charge carrier wave functions' overlap make the exciton-exciton interaction repulsive. Interestingly this behavior is appropriate for building QD laser based on the principle of amplified stimulated emission (ASE). The first such system reported is colloidal type-II (CdTe/CdSe) material where the band offsets allow the electron to be located in the shell CdSe and the hole in the core CdTe. Moreover, the spatially indirect valance (CdTe) to the conduction band

(CdSe) transition affects the absorption and emission wavelengths to be red-shifted compared to pure CdTe. Thus, it is possible even to emit wavelengths not accessible with core and shell materials and the emission was achievable up to 1000 nm.

Klimov et al. studied CdS/ZnSe core–shell nanoparticles in detail and successfully demonstrated their use for ASE (Klimov et al. 2007). The first observation is that shorter emission wavelengths compared to the band gaps of core and shell materials (CdS = 2.5 eV; ZnSe = 2.7 eV). The initial emission spectrum has two components assigned to a very fast decay of doubly excited particles and to a long-lived decay of singly excited particles. The difference between these two transitions is about 100 meV, having a doubly excited transition shifted toward higher energies. Both findings can be correlated to the type-II structure. On the contrary, in type-I nanocrystals where the electrons and holes are constrained in the same space, the exciton-exciton interactions are typically weak and attractive. This provides the doubly excited transition small shift toward lower energies.

The ASE behavior on examination yields some interesting features. Type-I materials can produce ASE at the doubly excited transition wavelength, while the type-II materials produced ASE at the central emission wavelength originating from the singly excited transition. Due to this effect, the type-II systems have a lower pump energy threshold for ASE compared to type-I systems. Consequently, this conduct makes type-II CSQD materials favorable candidates for laser development (Sect. 19.11.5).

19.9.4 Synthesis of Core–Shell QDs

Core–shell QDs can be synthesized involving a two-stage process where the first stage produces core QDs and the second stage makes the shell. We have already dealt in detail the synthesis of core QDs in Sects. 19.3, 19.4, and 19.5. The material and its thickness are two critical parameters for growing the shell. As for the material, generally, semiconductors are chosen for the core and shell with minor lattice mismatch. This mismatch is kept nominal to avoid lattice strain and defect states. These defect states are responsible for trapping the charge carrier and detrimental in lowering PL QY.

Next, the thickness of the shell material decides the effectiveness of the surface passivation. While thin shell material may lead to inadequate passivation, the thicker ones are likely to produce more defect states arising from lattice strain. Using the following simple scheme, the proper shell thickness can be estimated. First, the shell material volume, V_{shell} is calculated for the deposition of "m" monolayers of shell thickness:

$$V_{\text{shell}} = \frac{4}{3}\Pi\left[(r_c + m \times d_{\text{ML}})^3 - r_c^3\right]$$

Table 19.2 Important parameters for bulk II–VI semiconductors

Semiconductor	Structure (300 K)	E_{gap} (eV)	Density (g cm^{-3})	Lattice parameter (A^0)
CdTe	Zinc blende	1.43	5.870	6.48
CdSe	Wurtzite	1.74	5.810	4.3/7.01
ZnTe	Zinc blende	2.39	5.636	6.104
ZnSe	Zinc blende	2.69	5.266	5.668
CdS	Wurtzite	2.49	4.820	4.136/6.714
ZnS	Zinc blende	3.61	4.090	5.41

where r_c is the core radius and one monolayer shell thickness is d_{ML} expressed in nm.

Knowing V_{shell}, the material n_{shell} in moles is assessed for depositing "m" mL shell

$$n_{shell} = \frac{V_{shell} \times D_{core} \times N_A \times n_{QD}}{MW_{core}}$$

where MW_{core} and D_{core} are the molecular weight and density of the core material, N_A is the Avogadro number, and n_{QD} represents core QDs in solution in moles

After estimating the required shell thickness, successive ionic layer adsorption and reaction (SILAR) technique is employed for deposition. This technique involves careful introduction of anionic and cationic precursors into the core solution and one monolayer is deposited at a time. Repeating the above procedure, the requisite number of monolayers can be deposited on the core QDs' surface. Core–shell QDs having monodispersity and high luminescence yield are obtained by this technique.

A list of important material parameters is given in Table 19.2 for some useful bulk II–VI semiconductors.

19.9.5 Hydrothermal Process for CdSe–CdTe Core–Shell QDs

A two-stage hydrothermal process (Ramalingam et al. 2022) is used to prepare CdSe–CdTe QDs where CdSe nanoparticles are prepared first and then added to the precursors of CdTe. The materials required are (i) cadmium nitrate tetrahydrate ($Cd(NO_3)_2{\cdot}4H_2O$), (ii) sodium selenite (Na_2SeO_3), (iii) hydrazine hydrate ($N_2H_4{\cdot}H_2O$), and (iv) ammonia ($NH_3{\cdot}H_2O$).

Aqueous solutions of cadmium nitrate tetrahydrate and sodium selenite were made separately. The Cd^{2+} ion in cadmium nitrate solution was converted into Cd $(NH_3)_4{}^{2+}$ ion by treating with ammonia. On the other hand, Na_2SeO_3 is dissociated

by mixing with hydrazine hydrate to produce hydrogen selenide (H_2Se) where the oxidation state of selenium changed to Se^{2-}. By mixing together these solutions, CdSe cluster is formed which is next added to the CdTe precursor solution prepared by the following method. The key precursor NaHTe is prepared freshly by mixing $NaBH_4$ with Te (2: 1 molar ratio):

$$4NaBH_4 + 2Te + 7H_2O \rightarrow 2NaHTe + Na_2B_4O_7 + 14H_2 \uparrow$$

Stoichiometric amount of $NaBH_4$ is transferred to an ice-chilled flask, followed by the addition of H_2O and Te powder. The black Te powder gets dissolved in sodium borohydride solution after 2 h of vigorous stirring, to produce sodium tetra borate ($Na_2B_4O_7$) as white precipitate and supernatant NaHTe. The pressure build-up from generated hydrogen is released carefully through a vent provided.

This freshly prepared NaHTe solution is used to dissolve cadmium nitrate tetrahydrate ($Cd(NO_3)_2{\cdot}4H_2O$) and then 1.2 g of L-cysteine ($C_3H_7{\cdot}NO_2S$) as a capping agent in 25 ml of deionized water and CdSe is added gradually. The overall reaction is represented as

$$NaHTe + Cd(NO_3)_2 4H_2O + CdSe \xrightarrow{L-Cysteine} CdSe - CdTe \downarrow + NaOH + N_2O \uparrow + 4H_2O + 2O_2 \uparrow$$

The solution is relocated in a teflon-lined autoclave and heated at 180 °C in an oven for six hours. Figure 19.23 illustrates the step-wise hydrothermal synthesis process of CSQD (Ramalingam et al. 2022).

The solution is transferred to a flask from the hydrothermal reactor. Under refluxing conditions (at 110 °C), different durations produced controllable sized

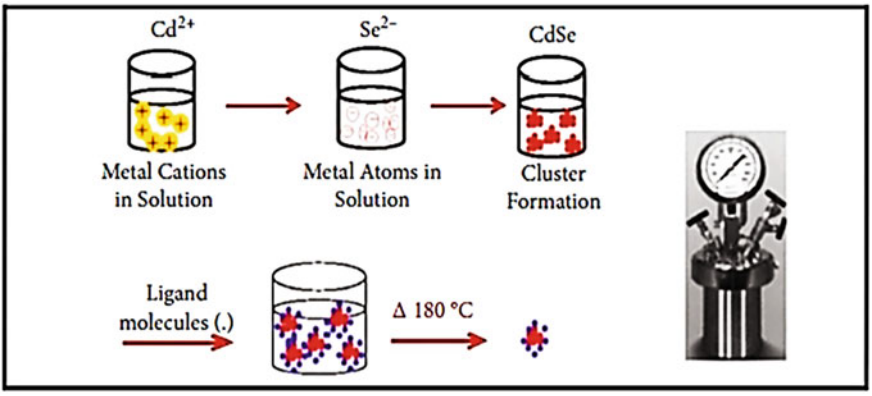

Fig. 19.23 Schematics of CdSe–CdTe quantum dots synthesis. Reproduced from De Gruyter Publications under Creative Common Licenses (Ramalingam et al. 2022)

CSQD. The refluxed solution is subjected to centrifuge and the precipitate is repeatedly washed with deionized water/ethanol. The precipitate was finally isolated using vacuum filtration and exposing it to 110 °C for three hours. The crimson-colored CdSe–CdTe core–shell QD obtained is characterized with XRD, SEM–EDX, TEM, and SAED techniques (Ramalingam et al. 2022). All these techniques are now regularly used for characterization of QDs and CSQDs.

19.10 Characterization of Core–Shell QDs

As-prepared nanocomposites are characterized with powder XRD patterns with nickel-filtered (monochromatic) CuKα radiation (1.5406 Å with a 0.02°/s scanning rate). Morphology of the materials is obtained using a scanning electron microscope (SEM) and energy-dispersive X-ray analyzer (EDX). Microscopic images of nanostructures is obtained through a transmission electron microscope (TEM, 200 kV acceleration voltage). Additionally, selected area electron diffraction pattern (SAED) is recorded with a 120 cm camera. UV–Vis–NIR spectrometer (200–900 nm) is used to characterize the absorption spectrum of the nanocomposite while the emission spectrum is obtained using a spectrometer (300–600 nm) with 380 nm as excitation wavelength.

19.10.1 X-Ray Diffraction (XRD) Studies

Nanocomposites are characterized by powder XRD technique with nickel-filtered (monochromatic) CuKα radiation (Fig. 19.24) (Ramalingam et al. 2022).

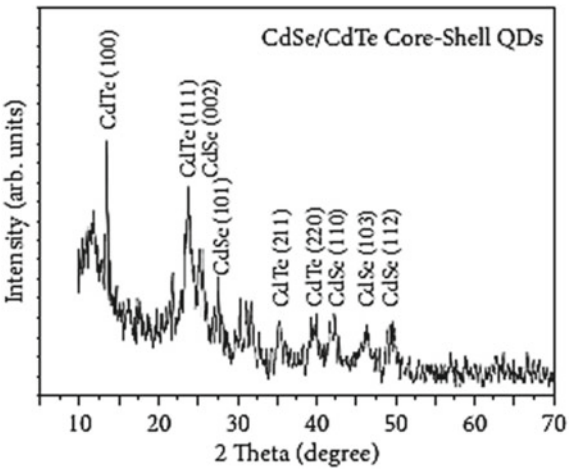

Fig. 19.24 XRD patterns of CdSe–CdTe CSQD. Reproduced from De Gruyter Publications under Creative Common Licenses (Ramalingam et al. 2022)

XRD patterns revealed the synthesis of hexagonal CdSe and cubic CdTe polycrystalline compounds. CdSe hexagonal phase formation is characterized by the peaks at 24.19° (002 plane), 27.62° (101 plane), 42.28° (112 plane), and 56.95° (002 plane). The other recorded peaks at 13.70, 24.19, 35.38, and 39.87° are due to CdTe cubic phase (100, 111, 211, and 220 planes). The diffraction peaks are matched with standard literature corresponding to CdTe and CdSe, respectively. The constrained particle size is reflected in wider signature peaks. Interestingly, even when CdSe is enclosed by CdTe, the diffraction peaks of CdSe cubic structure can be recognized. Williamson-Hall method can be used to find the size (D) and the induced strain (ε):

$$\beta \cos\theta = \frac{K\lambda}{D} + 4\varepsilon \sin\theta,$$

where λ is the wavelength of the X-ray used, β is the intensity FWHM, θ is Bragg's angle, and K is the shape factor. Using this formulation, the estimated 12.6 nm grain size of CdSe/CdTe confirmed the formation of a quantum dot. Further, SEM–EDX and TEM measurements revealed the shape and presence of the compositional elements.

19.10.2 SEM–EDX Analysis

Figure 19.25a presents the SEM image of CdSe–CdTe CSQD (Ramalingam et al. 2022). The monodispersed spherical nanoparticles are found without agglomeration. TEM analysis provides the precise measurement of the QD size and uniform particle size (10–20 nm) was found from the surface morphology. The EDX spectrum (Fig. 19.25b) indicates the presence of elemental Cd, Se, and Te in the QD. The result of the high weight and atomic percentage of Cd (shown in the Fig. 19.25b) indicate that both Se and Te are bonded to Cd.

19.10.3 TEM Analysis

Figure 19.26a–e represent the TEM images of CdSe–CdTe CSQDs (Ramalingam et al. 2022). The TEM images (@50–100 nm scale) (Fig. 19.26a, b) are indicative of vastly monodispersive and spherical nanoparticles. Further magnifications (@20 nm scale) (Fig. 19.26c) show the accurate particle size (~8–10 nm), which corroborates the XRD and SEM observations.

At higher magnifications, the TEM morphology and SEM morphology corroborates each other showing freestanding particle. The employed capping agent L-cysteine aided in size tuning of QDs and also refining the agglomeration. With higher magnifications (@5 nm scales), the surface indicates the unification of two crystal

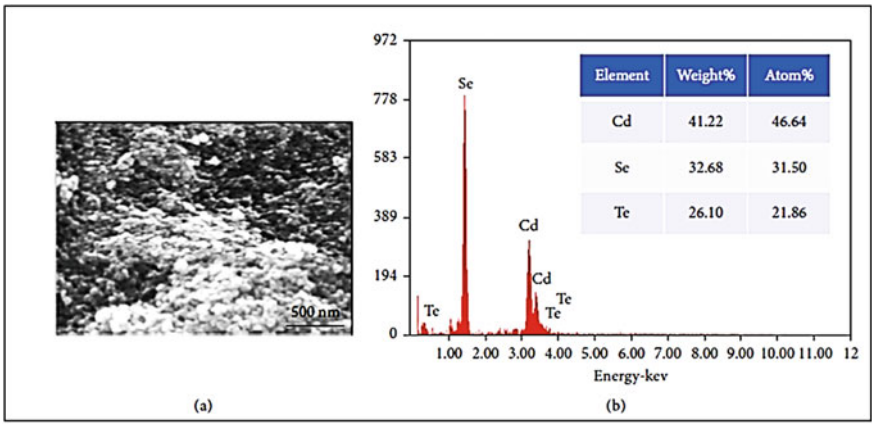

Fig. 19.25 **a** SEM morphology and **b** EDX spectrum of CdSe/CdTe. Reproduced from De Gruyter Publications under Creative Common Licenses (Ramalingam et al. 2022)

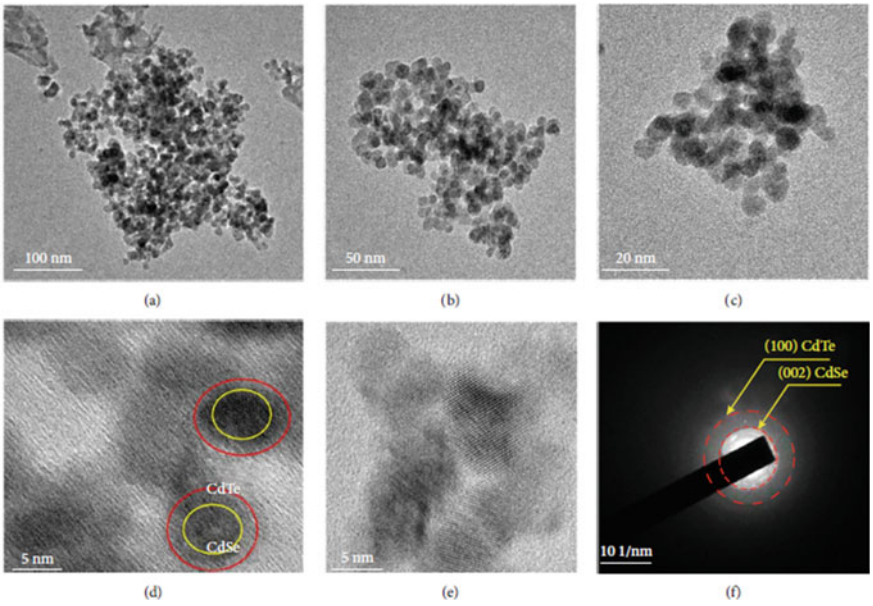

Fig. 19.26 TEM images (**a**–**e**) and SAED pattern (**f**) of CdSe/CdTe CSQD. Reproduced from De Gruyter Publications under Creative Common Licenses (Ramalingam et al. 2022)

structures probably due to CdSe QDs encircled with CdTe QD patches (Fig. 19.26d, e). In Fig. 19.26d, the CdSe surface and covering compound CdTe are shown by circles.

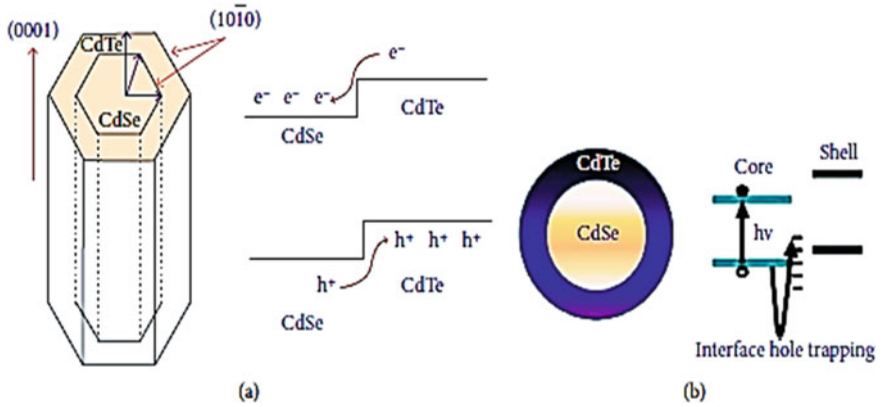

Fig. 19.27 Growth orientation (**a**) and electron–hole trapping (**b**) at the interface of CdSe–CdTe CSQD. Reproduced from De Gruyter Publications under Creative Common Licenses (Ramalingam et al. 2022)

These heterojunction CSQDs have significant advantages when effective exciton production/dissociation is combined with transporting separated charge carriers through discrete channels. It is now feasible to make heterojunction CSQDs with atomic-level control for efficient photovoltaic applications. The core and shell components are recognized by recording the SAED pattern shown in Fig. 19.26f. The inner and outer circular regions are ascribed to the CdSe (002) plane and CdTe (100) plane respectively. Further growth orientation of CdSe–CdTe CSQDs and electron–hole trapping at the interface is schematically presented in Fig. 19.27a, b (Ramalingam et al. 2022). The nonpolar interfaces (1010) of the surface facet are guided toward the wurzite (0001) direction as shown in Fig. 19.27a; the figure also shows the trapping of a fraction of holes at the CS interface (Fig. 19.27b).

19.10.4 Optical Absorption and Photoluminescence (PL)

Figure 19.28 represents the absorption and emission spectra of CdSe–CdTe QDs (Ramalingam et al. 2022). The absorption spectra (200–800 nm) consists of an excitonic peak at 560 nm and photoluminescence peak at λ_{emi} ~ 585 nm. When the PL maximum is nearer to its absorption onset, an increase in emission is observed owing to the direct recombination of HOMO and LUMO charge carriers. The CdSe–CdTe QDs obey type II characteristics and the observed optical absorption together with PL emission conforms the exciton nature of the type II material.

The observed emission in the λ_{emi} ~ 560–590 nm range arises due to several structural defects in the CSQD material. The plausible reason for the emission is due to the significant surface-to-volume (S/V) ratio, which normally creates interstitials and vacancies resulting in trap level. PL intensity is boosted due to low-concentration

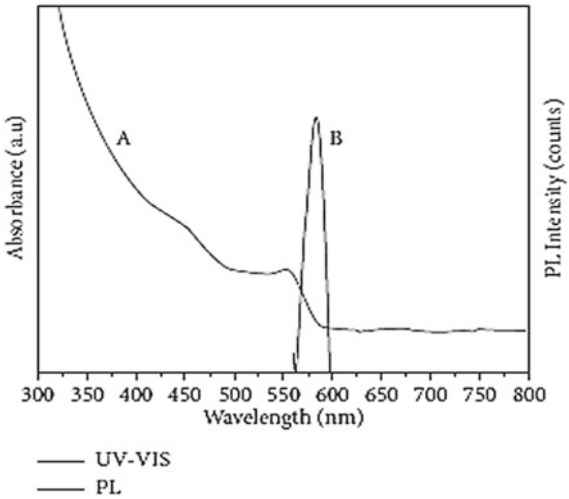

Fig. 19.28 CdSe–CdTe CSQDs: (A) Optical absorption and (B) PL spectrum. Reproduced from De Gruyter Publications under Creative Common Licenses (Ramalingam et al. 2022)

CdTe doping, where radiative recombination takes place at extra centers of CdSe. Three different phenomena are considered based on the optical properties: (i) reduced strain at the graded situations, (ii) lower defect concentration at the interface, and (iii) charge transfer cascading. These factors enhance the charge separation yield and charge carrier mechanism, which are utilized in photovoltaic device to enhance its efficiency (Ramalingam et al. 2022). Of late, some energy storage devices have started incorporating electrodes made with similar uniform spherical CdSe–CdTe CSQDs.

19.11 Applications of Core–Shell QDs

Currently, these CSQDs having excellent properties like size selected bandgap tunability, large PL having narrow FWHM, extended lifetime of excited-state, and good stability are being utilized for numerous applications. Some selected areas like solar cells, light-emitting diodes (LEDs), and biomedical applications will be dealt with in detail in the following sections.

19.11.1 Solar Cells

Quantum dots have revolutionized the area of making efficient solar cells. The traditional solar cell relies on sunlight photon knocking electrons out of a semiconductor into a circuit and producing electric power. However, the process efficiency is quite

low, which can be enhanced (typically 10% more efficient) by producing more electrons (or holes) for each solar photon that strikes QD materials. QD devices offer the added advantage of miniaturization in applications like CCDs (charge-coupled devices) and CMOS sensors.

In the initial developments, various QDs such as II–VI (CdSe, etc.) and IV–VI (PbSe, etc.) materials are employed as sensitizers in making the solar cell (Klimov 2006). However, as pointed out earlier, core–shell QDs offer superior qualities of controllable bandgap tunability along with photo-bleaching stability. Presently, type II material provides better cell efficiency though all three types of CSQDs are in use for various solar cell fabrication.

The QD-sensitized solar cell comprised of photo anode, counter electrode, and liquid electrolytes (Fig. 19.29a) (Pan et al. 2018). The photoanode is made of fluorine or indium-doped tin oxide (FTO or ITO) glass on which deposited a large bandgap semiconductor (ZnO, or TiO_2, etc.) material serving as a light absorber. Basically, solar photon excitation produced the charge carriers, i.e., electrons in the conduction and holes in the valance band of the QD. Then, the electrons are quickly introduced into the conduction band of TiO_2 and transported to the counter electrode via the FTO substrate. Meanwhile, reduced species of redox couple in the electrolyte neutralize the oxidized QD while the oxidized species of redox couple get reduced by the electrons from the counter electrode. The resulting photocurrent is measured via an external circuit. With the help of the characteristic J–V curve and the equation below, the power conversion efficiency (PCE) is calculated:

$$\mathrm{PCE} = \frac{I_{\mathrm{mp}} \cdot V_{\mathrm{mp}}}{P_{\mathrm{in}}} = \frac{J_{\mathrm{sc}} \cdot V_{\mathrm{oc}} \cdot \mathrm{FF}}{P_{\mathrm{in}}}$$

where P_{in} is incident power density, I_{mp} and V_{mp} are photocurrent and photovoltage, V_{oc} is the open-circuit voltage, J_{sc} is the short-circuit density, and FF represents the fill factor given by the ratio of specific value P_{max} to V_{oc} and J_{sc} (Fig. 19.29b) (Pan et al. 2018).

First use of core–shell QDs (inverted type I CdS-CdSe) as a sensitizer in solar cell was reported in 2009 (Lee and Lo 2009) where PCE value of 4.22% was obtained. After this, a large number of CSQDs are employed in the fabrication of the solar cell. Following years witnessed a new class of solar cells employing type I CdSe–ZnS CSQDs to sensitize TiO_2, where significantly improved stability of photo anode is reported. Improved PCE to the level of 9.48% was achieved using a novel type I CdSeTe/ZnS CSQDs, which is better than bare CdSeTe QD (8.02%) (Yang et al. 2015).

Further development occurred with the utilization of type II ZnSe/ZnS CSQDs. Due to the better charge separation process, it registered a high PCE efficiency. Synthesis of alloys like $CdSe_xTe_{1-x}$/CdS core–shell QDs by microwave-aided aqueous method produced 5.04% PCE. PCE was enhanced to 6.76% by sensitizing

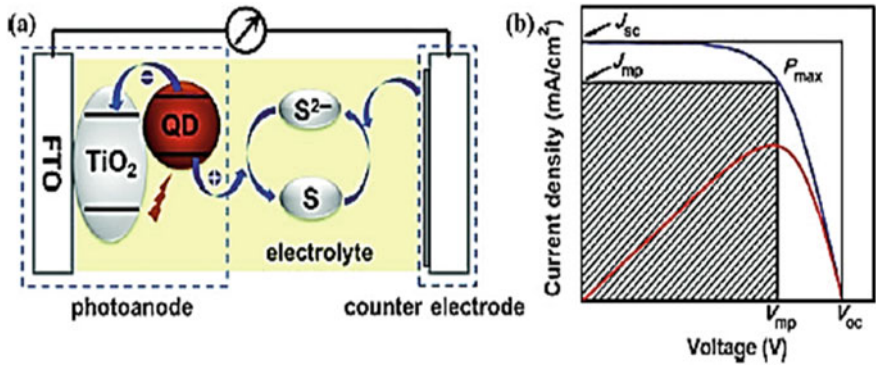

Fig. 19.29 QD-sensitized solar cells (**a**) typical *J*–*V* graph (**b**). Reprinted with permission from RSC Publications (Pan et al. 2018)

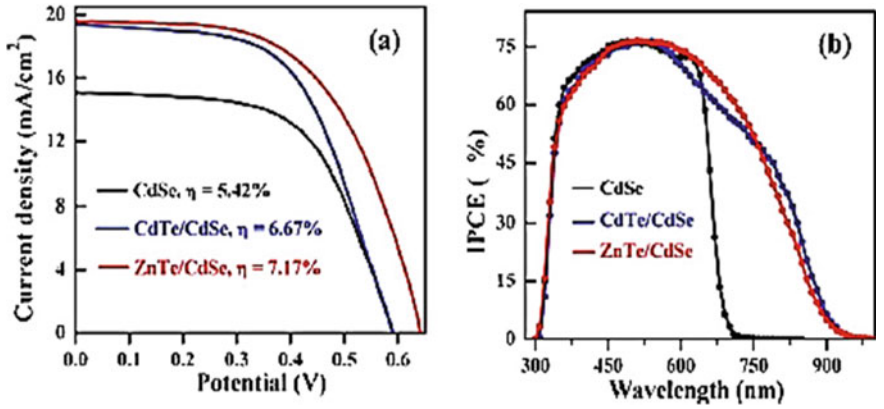

Fig. 19.30 Comparative performances of three types of solar cells based on CdSe QD, ZnTe/CdSe, and CdTe/CdSe CSQD: **a** *J*–*V* characteristics and **b** IPCE characteristics. Reprinted with permission from RSC Publications (Jiao et al. 2015)

with CdTe/CdSe CSQDs and further to 7.17% by employing ZnTe/CdSe CSQDs, both type II materials (Fig. 19.30) (Jiao et al. 2015).

19.11.2 Light-Emitting Diodes (LEDs)

Quantum dots offering several important advantages, are quickly put to use into computer screens and displays. The typical liquid crystal display (LCD) produces the image made by tiny red, blue, and green crystals. They perform as color filters which can be switched off and on using electronic control and they are also illuminated by a

bright backlight. However, QD-based displays look much more realistic and energy efficient since the quantum dots' color can conveniently be tuned and they do not need any backlight. These advantages are important in fabricating portable devices like mobiles where robust battery life is needed. Further quantum dots being much smaller than liquid crystals, they provide a much higher resolution image. It may be mentioned that since the brightness of typical quantum dots is higher compared to organic LEDs (OLEDs), they will possibly replace OLED displays as well. Summing up, QDs can be employed to make brighter TV screens with accurate colors of red, green, and blue pixels than in traditional LCD or competing OLED screens.

Presently, LED based on QDs (QLEDs) have gained much attention for its superior brilliance (~200 kilo cd m^{-2}), color purity (fwhm < 30 nm), and small working voltage (<2 V). The QLEDs are built with components like cathode, anode, QD films, electron/hole transport layers (ETL/HTL) (Fig. 19.31) (Choi et al. 2018). Applying a potential between the electrodes, electrons, and holes are introduced into ETLs and HTLs. Additionally, the charge carriers introduced into the QDs undergo radiative recombination. Above-charge transport materials (ETL/HTL) are crucial for the stability and efficient performance of QLEDs.

QLEDs normally use type I CSQDs because of their broader bandgap shell material confining the exciton and also minimizing surface defect states. This leads to increased quantum efficiency due to better PL QY and stable QD. It may be noted such enhanced PL QY not necessarily indicative of its electroluminescence (EL) performance. Detrimental processes like Augur recombination and inter-particle energy transfer are dominant with the interface structure and thus modification of structure becomes a critical issue (Choi et al. 2018). Better EL performance has been obtained with an enriched intermediate shell of ZnSe or CdS for CdSe/ZnS structure.

Highly stable QD with desired blinking properties can be made either by thick shell or multi-shell coverage on the QDs. This procedure enhanced PL QY and efficient suppression of the charge instability leading to superb device performance.

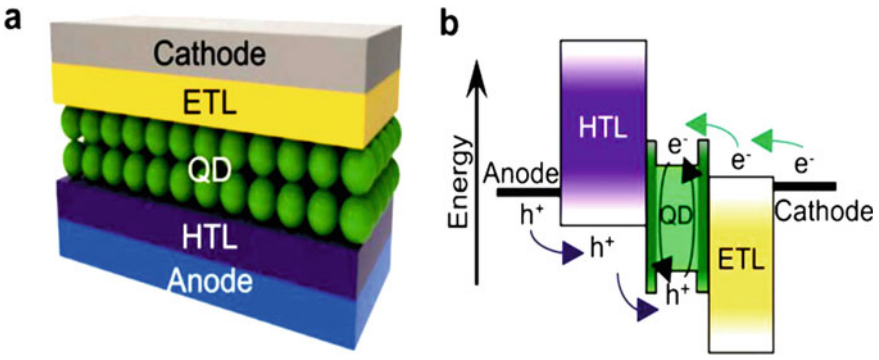

Fig. 19.31 **a** QLEDs device structure **b** energy-level illustration depicting charge introduction scheme. Reproduced from Springer Nature under Creative Common Licenses (Choi et al. 2018)

Recently, excellent green luminescent CdSe/ZnS CSQDs have been made employing a thick ZnS shell covering CdSe (Hao et al. 2019).

19.11.3 Optical Switching and Optical Limiting

It has been pointed out that quantum confinement makes QDs a potential third-order nonlinear optical materials (NLO). In recent times, CdSe QDs, have attracted attention in applications like optical switching and optical limiting. These effects are demonstrated using Z-scan measurement carried out with 532 nm nanosecond laser (Valligatla et al. 2016). It showed that at lower intensities, saturable absorption (SA) dominates while higher intensities recorded reverse saturable absorption (RSA). The SA is essentially ascribed to bleaching of the ground state and RSA arises due to free carrier absorption (FCA) of CdSe QDs.

Figure 19.32 presents the intensity-dependent open-aperture Z-scan curves of CdSe QDs in the input intensities (532 nm) ranging from 90 to 450 MW/cm^2 (Valligatla et al. 2016). It can be seen that in the range of 90–140 MW/cm^2, the SA becomes stronger with a concomitant broad Z-scan curve. Increasing the intensity further, RSA becomes dominant with a decrease in the transmittance. Under such intense excitation, resonant second photon absorption takes place lifting the excited electron in the conduction band to a still higher conduction band level. This process is known as free carrier absorption (FCA), which contributes to RSA. Thus, at higher intensities, SA of lower excited states competes with FCA resulting in RSA over SA.

Thus, the optical limiting behavior in working with nanosecond lasers depends on both FCA and thermal nonlinearities. This performance is utilized in mode-locking laser systems as saturable absorption at lower intensities while based on RSA behavior at high intensities. Therefore, CdSe QDs can have many applications like optical pulse compression, optical switching, and optical pulse narrowing. Extending the open aperture Z-scan studies of nanosecond laser to picosecond regime, a similar shift of SA to RSA is observed. In nanosecond laser excitation, contribution arises from thermal nonlinearities while electronic contribution with picosecond laser excitation. It may be worth pointing out that signs of nonlinearities owe to their origins such as a negative sign for thermal and a positive sign for electronic contribution. It is also found that optical nonlinearities tend to be always higher in nanosecond compared to pico-second laser excitations (Valligatla et al. 2016).

19.11.4 Optical Gain and Lasing

Investigation of optical gain in QDs led to a key development in demonstrating laser action in such a medium. With size-tunable quantum dots, stimulated emission with sufficient gain can be achieved at convenient wavelengths. With continued R&D in this area, QDs are now routinely synthesized comprising 100–10,000 atoms, having

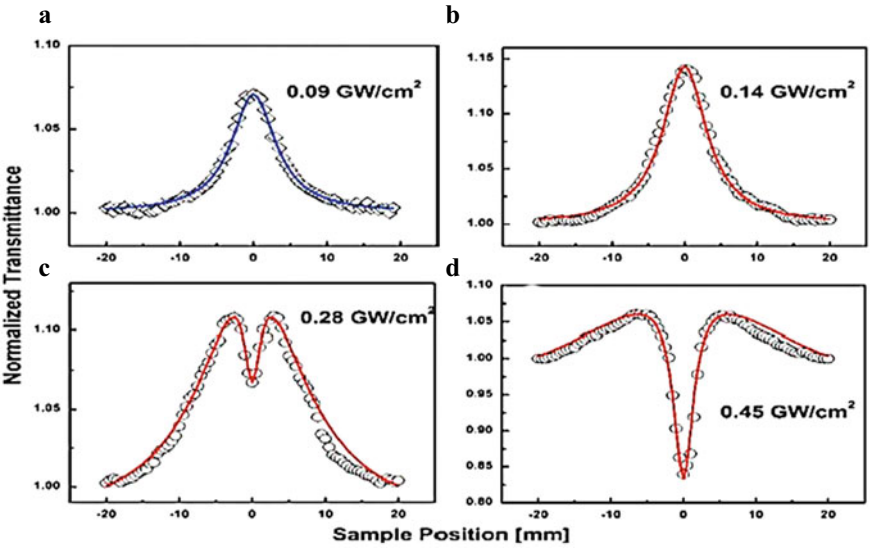

Fig. 19.32 Nonlinear absorption curves of CdSe QDs as a function of intensities of 532 nm nanosecond laser. Reproduced with permission from Elsevier Publications (Valligatla et al. 2016)

various sizes (1–10 nm), shapes (spherical, elongated, hollow, branched, etc.), and compositions (IV, II–VI, I–III–VI, I–II–VI–VI group materials). Such custom-made CSQDs are getting a lot of attention for development of active medium of micro-laser. Critical parameter for the achievement of laser action is to boost the optical gain determined by the difference in rates of absorption and stimulated emission. Recently, extensive investigations are being pursued on colloidal nanocrystals for laser development.

High performance and stable optical gain media have been worked out using tailored CdSe core (spherical; 2.4 nm) and CdS shell (rod; 39 nm) QDs and one- or two-photon pumping schemes. The attractive feature of such a configuration is to obtain tunable laser radiation by controlling the core and shell dimensions. Moreover, the 39 nm long nanorod shell provides a 2–4 times higher two-photon absorption cross-section compared to spherical CSQD. It may be even possible to achieve a still higher two-photon absorption cross-section by optimizing the dimensions and composition of CSQDs. Nanorods are capable of two-photon pumped lasing action even using a spherical optical cavity. Such smart engineering of heterostructures, in turn, offers promising opportunities for application in more areas. With these exciting developments, CSQDs are placed at the center stage of nanotechnology and are eloquently employed for making newer nanodevices using II–VI group compounds, particularly CdSe and CdTe.

19.11.5 Colloidal Quantum Dot Laser (Park et al. 2021)

For spherical QD particles having radius R, the quantum confinement-induced shift of its band gap is given by $\Delta E_{\text{conf}} = E_g - E_{g,\text{bulk}}$, where $E_{g,\text{bulk}}$ is the band gap of the bulk material and is proportional to R^{-2}. The size-dependent band gap permits easy tuning of the emission wavelength, which has been utilized in televisions and displays based on colloidal quantum dot (CQD). Proof-of-principle investigations have been carried out about 20 years back when CQD lasing was demonstrated (Park et al. 2021). Presently, CQD nanostructures are being used as commercial-grade optical and optoelectronic materials to build various devices like TVs, displays, and luminescent sunlight collectors. Researchers are now working to beat the non-radiative Auger recombination for the development of CQD laser. Let us now have a look at the working of CQD laser.

Light amplification in strongly confined CQDs resembles a simple 2-level system having a pair of electrons with opposite spins in its valence band (VB) state (Fig. 19.33) (Klimov et al. 2000). An exciton (single e–h pair) is generated by exciting an electron into the conduction band (CB). Such a state is capable of emitting light but cannot amplify the radiation, since the probability of stimulated emission by the CB electron is the same as photon absorption by the remaining electron in the VB.

This situation is similar to "optical transparency" (Fig. 19.33, middle), however, CQD can amplify radiation when the second VB electron is also excited to the CB achieving the population inversion required for lasing action. In effect, CQD starts lasing when an appreciable fraction of the QDs produce biexcitons (two e–h pairs) (Fig. 19.33, right).

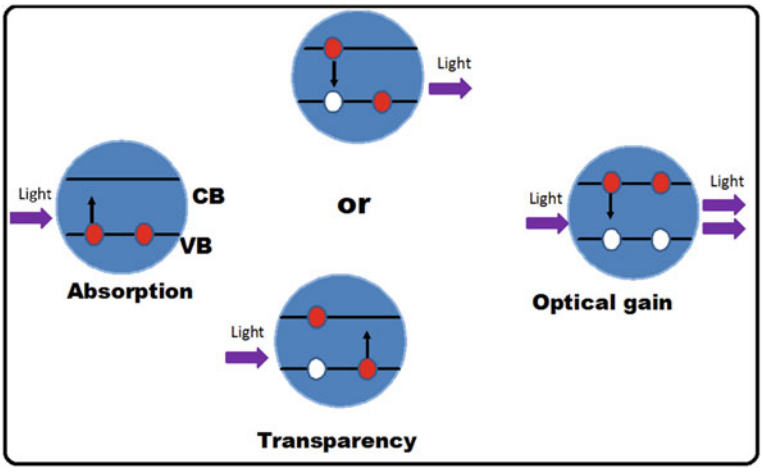

Fig. 19.33 Simple two-level description of CQD laser. When both electrons are excited into a biexcitonic state, the incident photon can induce stimulated emission. This is adapted from Springer Nature (Klimov et al. 2000)

Of late, two schemes have been employed to beat the Auger decay: (i) nonbiexcitonic mechanisms are single-exciton gain, implemented with type II CQDs, and (ii) charged-exciton gain, using photochemical or electrochemical CQD doping. The incentive is to effectively reduce the degeneracy of band-edge states so that biexcitons are not required to achieve optical gain.

Recent investigations have several demonstrations of direct control of Auger decay by making compositionally graded interiors of CQDs. It was implemented with continuously graded CQD material CdSe/Cd_xZn_{1-x} Se/$ZnSe_{0.5}$ $S_{0.5}$ which boosted the biexciton PL QYs to about 45%. Interestingly, Auger decay was heavily suppressed but still preserving large quantum confinement, with ΔE_{conf} of about 10 k_BT at room temperature. Further, R&D in Auger decay engineering led to the demonstration of optical gain with direct-current electrical pumping (Lim et al. 2018) for the first time.

Currently, CQDs are attracting attention as cheap and scalable optical-gain media. Further, recent insight and control of processes impeding light amplification have resulted in several breakthroughs. They are optically pumped cw laser, optical gain with dc-injection, and the demonstration of dual-function electroluminescent devices.

19.11.6 Biological and Chemical Applications

Quantum dots are making rapid strides in various medical fields like cancer treatments. Anti-cancer drugs bound to dots are made so that they get accumulated in particular parts of the body and deliver them. The big improvement over conventional drugs is that they can be precisely targeted at single organs such as liver, kidney, etc. This in effect reduces the undesired side effects associated with traditional chemotherapy.

Quantum dots are fast replacing organic dyes in medical applications as well. They can be used like nanoscopic light sources to illuminate and such color-specific cells can conveniently be studied under a microscope. Chemical and biological warfare agents such as anthrax can be detected using them. Unlike organic dyes, QDs produce a very bright desired color and are also photostable. Based on the knowledge of light dependence on plant growth, experiments have been undertaken using quantum dots to concentrate different colored lights for maximizing plants' growth.

Biological systems are quickly adopting the nanometric approach in their applications. Due to the similarity in size scales, appropriate QDs can be accurately designed and incorporated into many proteins having about tens of nm sizes. It is well known that biological systems being complex, their synthesis, structure, function, etc., are seldom understood in detail. Rational design of QD structures of the same size mimicking biological molecules will also provide a handle to probe and modify biological systems. Rapid entrance of nanostructures is taking place in the field of labeling, sensors, and drug delivery. In subsequent sections, detailed discussion will be made about some of their optical, biological, and chemical applications.

Around 1990, the QDs started playing a crucial role in biomolecular imaging, sensing, gene and drug delivery, and photodynamic therapy (Martynenko et al. 2017). QDs have many attractive features like size, surface chemistry, spectral properties, and finally, their stability. With all these features, they are being utilized for in-vitro and in-vivo detection/imaging in biological systems. While the parameters like emission wavelengths, stokes shift, and large absorption cross section can easily be controlled with changes in their size or composition, but their biocompatibility can be retained.

19.11.6.1 Biosensing

In medical science, with the help of specific biomarkers, it is possible for early detection/therapy of diseases and QDs are finding extensive use in such applications. Biosensing is done by looking at the quenching of QDs' luminescence. For example, investigations are carried out on heme iron absorption and clofazimine-protein interaction (Yang et al. 2016b) by employing core–shell biosensor. For this, Förster resonance energy transfer (FRET) scheme is employed with CdZnSeS/ZnS alloyed CSQD as energy donor. Alongside, another scheme is used by first capping of multifunctional polymer and followed by functionalizing with cyanine 3-labeled human serum albumin (HSA) (Yang et al. 2016b) known as the direct ligand method.

19.11.6.2 Gene and Drug Delivery

The medical applications recently have seen increased demand for gene and drug delivery. Many benefits are recognized by using drug-formulated QDs providing targeted drug delivery, better cellular uptake, and long lifetime. Various in-vivo and in-vitro studies have been made with new bioconjugated QDs (Matea et al. 2017). Recently, the drug paclitaxel (PTX) has been used for human cancer therapy with CdTe/CdS/ZnS core–shell QDs. The PTX drug loaded on ZnSe:Mn/ZnS CSQDs and hybrid silica nanocapsules are used for fluorescence imaging and chemotherapy (Zhao et al. 2017). Recently, antibacterial and anticancer nano-drugs have been developed by quercetin (QE)-loaded CdSe/ZnS CSQDs.

19.11.6.3 Therapy

Both in-vitro and in-vivo photodynamic therapy have seen enormous progress using QDs either alone or with efficient photosensitizers such as phthalocyanines, porphyrins organic dyes, inorganic complexes, etc. It may be noted that photodynamic therapy proceeds through singlet oxygen and various reactive oxygen

species (ROS) (Biju et al. 2010). Initially, it was found that QDs have poor efficiency in producing singlet oxygen, however, later ~70% enhancement in efficiency was obtained by conjugating choline e6 with QDs. But, further progress in bio-applications is stalled due to cytotoxicity of cadmium in QDs.

19.12 Summary and Future Prospects

The present overview provides a broad perspective for II–VI semiconductor CSQDs, especially their chemical synthesis and their prospective applications in solar cells, LEDs, biomedical, etc.

It is reasonably tough making forecasts of future technology. It is worth mentioning the way the quality of life improved worldwide with blue GaN LED for solid-state lighting. Further combining this LED with luminescent QDs led to another influential technology. These inexpensive and energy-efficient devices are capable of producing pure colors as well as broad-band white light. They are utilized both in macroscopic and microscopic scale area lighting with white LEDs (Osram) and micro-LEDs.

Future QD materials are best suited for high-quality pictures in TVs and monitors. QD technology started penetrating the TV market from 2015, and by 2018, the sale of QD TVs reached $18.7 million. The forecast indicates (Peach 2015) (Fig. 19.34) that QD technology will be adopted by 2025 for TVs (60%) and monitors (51%). Further, QDs have strategic use in defense or counter-espionage, by integrating QDs into dust to track enemies.

Two break-through application areas with QDs are worth revealing:

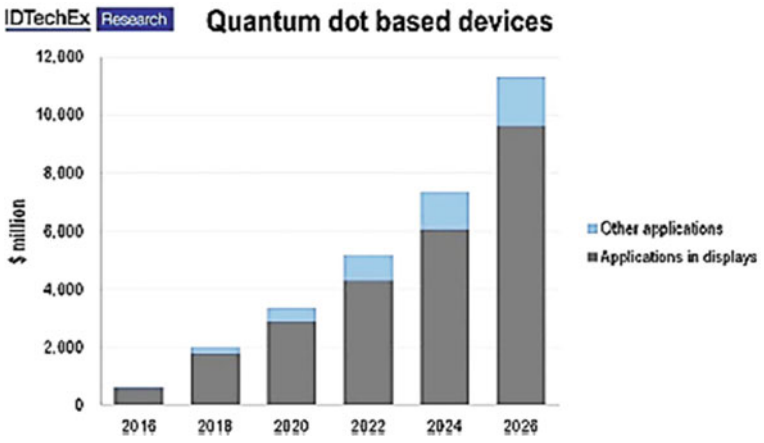

Fig. 19.34 Sale ($ million) forecast for QD devices/components during 2016–2026. Reproduced from Internal (Peach 2015)

Table 19.3 Li-Fi versus Wi-Fi technologies (Kaushik et al. 2017)

Item	Li-Fi	Wi-Fi
Speed	1–3.5 Gbps	54–250 Mbps
Range	10 m	20–100 m
Spectrum range	10,000 times than Wi-Fi	Radio spectrum range
Data transfer medium	Light used as carrier	Radio spectrum
Frequency band	100 THz	2.4 GHz
Safety	Non-hazardous	Hazardous

(a) Li-Fi Technology: With fast capabilities, LEDs, are being utilized in transferring data between computers. Li-Fi (Light Fidelity) technology uses visible light as the carrier in data transmission/networking, whereas Wi-Fi uses radio wavelength. Li-Fi is attractive as one futuristic technology where every bulb can be converted into a whole new Wi-Fi hotspot. With this innovation, information can be networked at a speed as fast as about 10 Gbps. It is contemplated that Li-Fi may be employed soon with its unique properties (Table 19.3) in aircraft, hospitals, and underwater communications (Kaushik et al. 2017).

(b) Quantum Information Science: Currently, the computers are getting faster and smaller with advanced technology, but eventually, the physical limits of materials will impede the activity, till we find completely different technologies. As already discussed one possibility is to store and transmit information with photons in place of electrons, i.e., the technology of photonics. It is knocking at the door to build optical computers using QDs in a similar way the present computers are built upon transistors for memory chips and logic gates. Optical computers are expected to be realized soon depending on the progress made by computer scientists. It may be pointed out that quantum computer works on quantum bits stored by "entangled" atoms, ions, electrons, or photons and they can work on different problems in parallel.

From our previous discussion on CQDs, it may be quite easy to incorporate either single QD or QD arrays. Current insight of such a system is continuously improving about their quantum coherent effects to use them as podiums for quantum information science. CQD designing has the flexibility to achieve control of quantum mechanical properties like charge and spin. Investigations are progressing at a fast rate for optically addressable qubits usable in quantum computation, simulation, and sensing.

Summarizing, R&D on QD is progressing at a great pace. It is working at the cross-roads of chemistry, physics, materials science, and engineering. Development in this area over the last 20 years has parallel in bulk semiconductor technology during mid-twentieth century. In the end, it may be mentioned that the halide perovskite QDs are the latest entrant having many more promising features. Researchers all over the world are hopeful in mitigating the cytotoxicity issue of cadmium, lead, etc.; these small wonders will have endless frontiers.

Acknowledgements The author acknowledges the works of numerous researchers in this field and apologies for omitting many other works. He is indebted to his brother Prof. Salil K. Sarkar, Presidency University, Kolkata for encouragement to work in this subject area. He is also grateful to the Department of Atomic Energy and Bhabha Atomic Research Center for the persistent support provided for his research activities.

References

Abe, S., Capek, R.K., Geyter, B.D., Hens, Z.: Reaction chemistry/nanocrystal property relations in the hot injection synthesis, the role of the solute solubility. ACS Nano **7**, 943–949 (2013)

Amirav, L., Amirav, A., Lifshitz, E.: A spray-based method for the production of semiconductor nanocrystals. J. Phys. Chem. B **109**, 9857–9860 (2005)

Bang, E., Choi, Y., Cho, J., Suh, Y.H., Ban, H.W., Son, J.S., Park, J.: Synthesis of micro and nanostructures in microfluidic systems. Chem. Soc. Rev. **39**, 1183–1202 (2010)

Bang, E., Choi, Y., Cho, J., Suh, Y.H., Ban, H.W., Son, J.S., Park, J.: Large-scale synthesis of highly luminescent InP@ ZnS quantum dots using elemental phosphorus precursor. Chem. Mater. **29**, 4236–4243 (2017)

Bera, D., Qian, L., Tseng, T.K., Holloway, P.H.: Quantum dots and their multimodal applications: a review. Mater. (basel) **3**, 2260–2345 (2010)

Biju, V., Mundayoor, S., Omkumar, R.V., Anas, A., Ishikawa, M.: Bioconjugated quantum dots for cancer research: present status, prospects and remaining issues. Biotechnol. Adv. **28**, 199–213 (2010)

Bobo, D., Robinson, K.J., Islam, J., Thurecht, K.J., Corrie, S.R.: Nanoparticle-based medicines: a review of FDA-approved materials and clinical trials to date. Pharm. Res. **33**, 2373–2387 (2016)

Brown, R.G.W., Pike, E.R.: A history of optical and optoelectronic physics in the twentieth century. In: Brown, L.M., Pais, A., Pippard, B. (eds.) Twentieth Century Physics, vol. III. American Institute of Physics Press, New York, USA (1995)

Choi, M.K., Yang, J., Hyeon, T., Kim, D.H.: Flexible quantum dot light-emitting diodes for next-generation displays. npj Flex. Electron. **2**, 10 (2018). https://doi.org/10.1038/s41528-018-0023-3

Dai, X., Deng, Y., Peng, X., Jin, Y.: Quantum-dot light-emitting diodes for large-area displays: towards the dawn of commercialization. Adv. Mater. **29**, 1607022 (2017)

Efros, A.L., Brus, L.E.: Nanocrystal quantum dots: from discovery to modern development. ACS Nano **15**, 6192–6210 (2021)

Ekimov, A.I., Onushchenko, A.A., Tsekhomski, V.A.: Exciton absorption by copper chloride crystal in glassy matrix. Fiz. Khim. Stekla **6**, 511–512 (1980)

Elias, J., Lévy-Clément, C., Bechelany, M., Michler, J., Wang, G., Wang, Z., Philippe, L.: Hollow urchin-like ZnO thin films by electrochemical deposition. Adv. Mater. **22**, 1607 (2010)

Feynman, R.P.: There's Plenty of Room at the Bottom. California Institute of Technology, Engineering and Science Magazine (1960)

Guleria, A., Singh, A.K., Rath, M.C., Sarkar, S.K., Adhikari, S.: The role of structural and fluidic aspects of room temperature ionic liquids in influencing the morphology of CdSe nano/microstructures grown in situ. Dalton Trans. **43**, 11843–11854 (2014)

Hao, J., Liu, H., Miao, J., Lu, R., Zhou, Z., Zhao, B., Xie, B., Cheng, J., Wang, K., Delville, M.H.: A facile route to synthesize CdSe/ZnS thick-shell quantum dots with precisely controlled green emission properties: towards QDs based LED applications. Sci. Rep. **9**, 12048 (2019)

Hines, M.A., Guyot-Sionnest, P.: Synthesis and characterization of strongly luminescing ZnS-capped CdSe nanocrystals. J. Phys. Chem. **100**, 468–471 (1996)

Huang, X., Tong, X., Wang, Z.: Rational design of colloidal core-shell quantum dots for optoelectronic applications. J. Electron. Sci. Technol. **18**, 100018 (2020)

Jiao, S., Shen, Q., Mora-Sero, I., Wang, J., Pan, Z., Zhao, K., Kuga, Y., Zhong, X., Bisquert, J.: Band engineering in core/shell ZnTe/CdSe for photovoltage and efficiency enhancement in exciplex quantum dot sensitized solar cells. ACS Nano **9**, 908–915 (2015)

Kamat, P.V.: Quantum dot solar cells. Semiconductor nanocrystals as light harvesters. J. Phys. Chem. C **112**, 18737–18753 (2008)

Kaushik, R., Jaiswal, R., Joon, R.: Light fidelity: a new prototype in wireless communication. Int. J. Innov. Res. Comput. Sci. Technol. **5**, 277–280 (2017)

Kikkeri, R., Laurino, P., Odedra, A., Seeberger, P.H.: Synthesis of carbohydrate-functionalized quantum dots in microreactors. Angew. Chem. Int. Ed. **49**, 2054–2057 (2010)

Klimov, V.I.: Mechanisms for photogeneration and recombination of multiexcitons in semiconductor nanocrystals: implications for lasing and solar energy conversion. J. Phys. Chem. B **110**, 16827–16845 (2006)

Klimov, V.I., Mikhailovsky, A.A., Xu, S., Malko, A., Hollingsworth, J.A., Leatherdale, C.A., Eisler, H.-J., Bawendi, M.G.: Optical gain and stimulated emission in nanocrystal quantum dots. Science **290**, 314–317 (2000)

Klimov, V.I., Ivanov, S.A., Nanda, J., Achermann, M., Bezel, I., McGuire, J.A., Piryatinski, A.: Single-exciton optical gain in semiconductor nanocrystals. Nature **447**, 441–446 (2007)

Lee, Y.-L., Lo, Y.-S.: Highly efficient quantum-dot-sensitized solar cell based on cosensitization of CdS/CdSe. Adv. Funct. Mater. **19**, 604–609 (2009)

Li, J.J., Wang, Y.A., Guo, W., Keay, J.C., Mishima, T.D., Johnson, M.B., Xiaogang, P.: Large-scale synthesis of nearly monodisperse CdSe/CdS core/shell nanocrystals using air-stable reagents via successive ion layer adsorption and reaction. J. Am. Chem. Soc. **125**, 12567–12575 (2003)

Liang-Shi, L., Jiangtao, H., Weidong, Y., Alivisatos, A.P.: Band gap variation of size- and shape-controlled colloidal CdSe quantum rods. Nano Lett. **1**, 349–351 (2001)

Lim, J., Park, Y.-S., Klimov, V.I.: Optical gain in colloidal quantum dots achieved with direct-current electrical pumping. Nat. Mater. **17**, 42–48 (2018)

Ma, Z., Yu, J., Dai, S.: Preparation of inorganic materials using ionic liquids. Adv. Mater. **22**, 261–285 (2010)

Martynenko, I.V., Litvin, A.P., Purcell-Milton, F., Baranov, A.V., Fedorov, A.V., Gun'ko, Y.K.: Application of semiconductor quantum dots in bioimaging and biosensing. J. Mater. Chem. B **5**, 6701–6727 (2017)

Matea, C.T., Mocan, T., Tabaran, F., Pop, T., Mosteanu, O., Puia, C., Iancu, C., Mocan, L.: Quantum dots in imaging, drug delivery and sensor applications. Int. J. Nanomedicine **12**, 5421–5431 (2017)

Mauro, E., Eva, P., Jordi, A., Nicolas, S., Thierry, P., Joan, R.M.: Capping ligand effects on the amorphous-to-crystalline transition of CdSe nanoparticles. Langmuir **24**, 11182–11188 (2008)

Mohamed, W.A.A., El-Gawad, H.A., Mekkey, S., Galal, H., Handal, H., Mousa, H., Labib, A.: Quantum dots synthetization and future prospect applications. Nanotechnol. Rev. **10**, 1926–1940 (2021)

Montanarella, F., Kovalenk, M.V.: Three millennia of nanocrystals. ACS Nano **16**, 5085−5102 (2022)

Murray, C.B.: Thesis, Massachusetts Institute of Technology, Cambridge, MA (1995)

Murray, C.B., Norris, D.J., Bawendi, M.G.J.: Synthesis and characterization of nearly monodisperse CdE (E = sulfur, selenium, tellurium) semiconductor nanocrystallites. J. Am. Chem. Soc. **115**, 8706–8715 (1993)

Novotny, L., Hecht, B.: Principles of Nano-Optics. Cambridge University Press, Cambridge, England (2006)

Optics and Photonics: Essential Technologies for Our Nation. National Academies Press, Washington DC, USA (2013)

Palomaki, P.: Quantum dots + OLED = Your next TV: formerly rival technologies will come together in new Samsung displays. IEEE Spectr. **59**, 52–53 (2022)

Pan, Z., Rao, H., Mora-Seró, I., Bisquert, J., Zhong, X.: Quantum dot-sensitized solar cells. Chem. Soc. Rev. **47**, 7659–7702 (2018)

Park, Y.-S., Roh, J., Diroll, B.T., Schaller, R.D., Klimov, V.I.: Colloidal quantum dot lasers. Nat. Rev. Mater. **6**, 382–401 (2021)
Peach, M.: QD Vision, Konka launch quantum dot TVs into China. https://www.optics.org/news/6/4/16 (2015). 2021
Peng, P., Milliron, D.J., Hughes, S.M., Alivisatos, A.P., Saykally, R.: Femtosecond spectroscopy of carrier relaxation dynamics in type II CdSe/CdTe tetrapod heteronanostructures. Nano Lett. **5**, 1809–1813 (2005)
Pietryga, J.M., Park, Y.-S., Lim, J., Fidler, A.F., Bae, W.K., Brovelli, S., Klimov, V.I.: Spectroscopic and device aspects of nanocrystal quantum dots. Chem. Rev. **116**, 10513−10622 (2016)
Prasad, K., Jha, A.K.: Biosynthesis of CdS nanoparticles: an improved green and rapid procedure. J. Colloid Interface Sci. **342**, 68–72 (2010)
Protesescu, L., Yakunin, S., Bodnarchuk, M.I., Krieg, F., Caputo, R., Hendon, C.H., Yang, R.X., Walsh, A., Kovalenko, M.V.: Nanocrystals of cesium lead halide perovskites ($CsPbX_3$, X = Cl, Br, and I): novel optoelectronic materials showing bright emission with wide color gamut. Nano Lett. **15**, 3692–3696 (2015)
Ramalingam, G., Ragupathi, C., Rangasamy, B., Colak, I., Vetrivelan, V., Poudineh, N., Balasubramani, R., Chang, S.W., Gengan, R.M.: Structural and optical properties of CdSe/CdTe core-shell quantum dots. J. Nanomater. 6316716 (2022). https://doi.org/10.1155/2022/6316716
Reiss, P., Protiere, M., Li, L.: Core-shell semiconductor nanocrystals. Small **5**, 154–168 (2009)
Rogach, A.L., Katsikas, L., Kornowski, A., Su, D., Eychmuller, A., Weller, H.: Synthesis and characterization of thiol-stabilized CdTe nanocrystals. Ber. Bunsen-Ges. Phys. Chem. **100**, 1772–1778 (1996)
Rossetti, R., Nakahara, S., Brus, L.E.J.: Quantum size effects in the redox potentials, resonance Raman spectra, and electronic spectra of CdS crystallites in aqueous solution. Chem. Phys. **79**, 1086–1088 (1983)
Shi, J., Kantoff, P.W., Wooster, R., Farokhzad, O.C.: Cancer nanomedicine: progress, challenges and opportunities. Nat. Rev. Cancer **17**, 20–37 (2017)
Shiang, J.J., Kadavanich, A.V., Grubbs, R.K., Alivisatos, A.P.: J. Phys. Chem. **99**, 17417–17422 (1995)
Singh, S., Rath, M.C., Singh, A.K., Sarkar, S.K., Mukherjee, T.: Reversible formation of CdSe nanoparticles in aqueous solutions by high-energy electron beam irradiation. Mater. Chem. Phys. **124**, 6–9 (2010)
Singh, S., Rath, M.C., Sarkar, S.K.: Investigation of dynamics of radiolytic formation of CdSe nanoparticles in aqueous solutions. J. Phys. Chem. A **115**, 13251–13258 (2011a)
Singh, S., Rath, M.C., Singh, A.K., Mukherjee, T., Jayakumar, O.D., Tyagi, A.K., Sarkar, S.K.: CdSe nanoparticles grown via radiolytic methods in aqueous Solutions. Rad. Phys. Chem. **80**, 736–741 (2011b)
Singh, S., Guleria, A., Rath, M.C., Singh, A.K., Adhikari, S., Sarkar, S.K.: Sea urchin like shaped CdSe nanoparticles grown in aqueous solutions via electron beam irradiation. J. Nanosci. Nanotechnol. **13**, 5365–5373 (2013a)
Singh, S., Singh, A.K., Rath, M.C., Adhikari, S., Sarkar, S.K.: Radiolytic synthesis and spectroscopic investigations of cadmium selenide quantum dots grown in cationic surfactant based quaternary water-in-oil microemulsions. J. Colloid Interface Sci. **398**, 112–119 (2013b)
Singh, S., Guleria, A., Rath, M.C., Singh, A.K., Adhikari, S., Sarkar, S.K.: Shape evolution of CdSe nanomaterials in microheterogeneous media. Adv. Mater. Lett. **4**, 449–453 (2013c)
Spinks, J.W.T., Woods, R.J.: An Introduction Radiation Chemistry, 3rd edn. Wiley, New York (1976)
Steckel, J.: Ph.D. Thesis, Massachusetts Institute of Technology, Cambridge, MA (2006)
Taniguchi, N.: On the Basic Concept of Nano-Technology. In: Proceedings of the International Conference on Production Engineering, pp. 5−10. Japan Society of Precision Engineering, Tokyo (1974)
Tong, X., Wang, Z.M. (eds.): Core-Shell Quantum Dots Synthesis, Properties and Devices. Springer Nature Switzerland AG (2020)

Valligatla, S., Haldar, K.K., Patra, A., Desai, N.R.: Nonlinear optical switching and optical limiting in colloidal CdSe quantum dots investigated by nanosecond Z-scan measurement. Opt. Laser Technol. **84**, 87–93 (2016). https://doi.org/10.1016/j.optlastec.2016.05.009

Vossmeyer, T., Katsikas, L., Giersig, M., Popovic, I.G., Diesner, K., Chemseddine, A., Eychmueller, A., Weller, H.J.: CdS nanoclusters: synthesis, characterization, size dependent oscillator strength, temperature shift of the excitonic transition energy, and reversible absorbance shift. J. Phys. Chem. **98**, 7665–7673 (1994)

Wang, A., Yan, X., Zhang, M., Sun, S., Yang, M., Shen, W., Pan, X., Wang, P., Deng, Z.: Controlled synthesis of lead-free and stable perovskite derivative Cs_2SnI_6 nanocrystals via facile hot-injection process. Chem. Mater. **28**, 8132–8140 (2016)

Yakoubi, A., Chaabane, T.B., Aboulaich, A., Mahiou, R., Balan, L., Medjahdi, G., Schneider, R.: Aqueous synthesis of Cu-doped CdZnS quantum dots with controlled and efficient photoluminescence. J. Lumin. **175**, 193–202 (2016)

Yang, J., Wang, J., Zhao, K., Izuishi, T., Li, Y., Shen, Q., Zhong, X.: CdSeTe/CdS type-I core/shell quantum dot sensitized solar cells with efficiency over 9%. J. Phys. Chem. C **119**, 28800–28808 (2015)

Yang, Z., Lu, L., Kiely, C.J., Berger, B.W., Mcintosh, S.: Biomineralized CdS quantum dot nanocrystals: optimizing synthesis conditions and improving functional properties by surface modification. Ind. Eng. Chem. Res. **55**, 11235–11244 (2016a)

Yang, H.Y., Fu, Y., Jang, M.S., Li, Y., Lee, J.H., Chae, H., Lee, D.S.: Multifunctional polymer ligand interface CdZnSeS/ZnS quantum dot/Cy3-labeled protein pairs as sensitive FRET sensors. ACS Appl. Mater. Interfaces **8**, 35021–35032 (2016b)

Yang, J., Choi, M.K., Yang, U.J., Kim, S.Y., Kim, Y.S., Kim, J.H., Kim, D.-H., Hyeon, T.: Toward full-color electroluminescent quantum dot displays. Nano Lett. **21**, 26–33 (2021)

Yen, B.: Ph.D. Thesis, Massachusetts Institute of Technology, Cambridge, MA (2007)

Zhao, T., Liu, X., Li, Y., Zhang, M., He, J., Zhang, X., Liu, H., Wang, X., Gu, H.: Fluorescence and drug loading proprieties of ZnSe:Mn/ZnS-paclitaxel/SiO2 nanocapsules templated by F127 micelles. J. Colloid Interface Sci. **490**, 436–443 (2017)

Zhou, Y., Zhao, H., Ma, D., Rosei, F.: Harnessing the properties of colloidal quantum dots in luminescent solar concentrators. Chem. Soc. Rev. **47**, 5866–5890 (2018)